Defense Nuclear Agency
Alexandria, VA 22310-3398

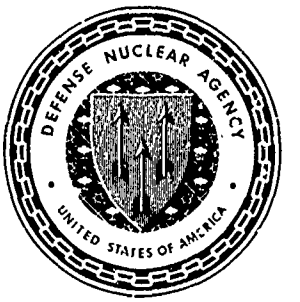

DNA-TR-89-157

Subthreshold Technique for Fixed and Interface Trapped Charge Separation in Irradiated MOSFETs

Edward W. Enlow
Ronald L. Pease
David R. Alexander
Mission Research Corporation
1720 Randolph Road SE
Albuquerque, NM 87106-4245

April 1990

Technical Report

CONTRACT Nos. DNAALO2-86-D-0043
and DNA-MIPR-89-500

Destroy this report when it is no longer needed. Do not return to sender.

PLEASE NOTIFY THE DEFENSE NUCLEAR AGENCY, ATTN: CSTI, 6801 TELEGRAPH ROAD, ALEXANDRIA, VA 22310-3398, IF YOUR ADDRESS IS INCORRECT, IF YOU WISH IT DELETED FROM THE DISTRIBUTION LIST, OR IF THE ADDRESSEE IS NO LONGER EMPLOYED BY YOUR ORGANIZATION.

DISTRIBUTION LIST UPDATE

This mailer is provided to enable DNA to maintain current distribution lists for reports. We would appreciate your providing the requested information

- ☐ Add the individual listed to your distribution list.
- ☐ Delete the cited organization/individual.
- ☐ Change of address

NAME: _____

ORGANIZATION _____

OLD ADDRESS	CURRENT ADDRESS
_____	_____
_____	_____
_____	_____

TELEPHONE NUMBER: (___) _____

SUBJECT AREA(S) OF INTEREST.

_____	_____
_____	_____
_____	_____

DNA OR OTHER GOVERNMENT CONTRACT NUMBER: _____

CERTIFICATION OF NEED-TO-KNOW BY GOVERNMENT SPONSOR (if other than DNA).

SPONSORING ORGANIZATION: _____

CONTRACTING OFFICER OR REPRESENTATIVE: _____

SIGNATURE: _____

CUT HERE AND RETURN

Director
Defense Nuclear Agency
ATTN. TITL
Washington, DC 20305-1000

Director
Defense Nuclear Agency
ATTN: TITL
Washington, DC 20305-1000

REPORT DOCUMENTATION PAGE

Form Approved OMB No 0704-0188

1. AGENCY USE ONLY *(Leave blank)*	2. REPORT DATE	3. REPORT TYPE AND DATES COVERED
	900401	Technical 870228 to 880310

4. TITLE AND SUBTITLE
Subthreshold Technique for Fixed and Interface Trapped Charge Separation in Irradiated MOSFETs

5. FUNDING NUMBERS
C - DNAAL02-86-D-0043
C - DNA-MIPR-89-500
PE - 62715H
PR
TA
WU

6. AUTHOR(S)
Edward W. Enlow, Ronald L. Pease, and David R. Alexander

7. PERFORMING ORGANIZATION NAME(S) AND ADDRESS(ES)
Mission Research Corporation
1720 Randolph Road SE
Albuquerque, NM 87106-4245

8. PERFORMING ORGANIZATION REPORT NUMBER
MRC/ABQ-R-1069

9. SPONSORING/MONITORING AGENCY NAME(S) AND ADDRESS(ES)
Defense Nuclear Agency
6801 Telegraph Road
Alexandria, VA 22310-3398
RAEE/Fore

Harry Diamond Labs.
2800 Powder Mill Road
Adelphi, MD 20783-1197

10. SPONSORING/MONITORING AGENCY REPORT NUMBER
DNA-TR-89-157

11. SUPPLEMENTARY NOTES

12a. DISTRIBUTION/AVAILABILITY STATEMENT
Approved for public release; distribution is unlimited.

12b. DISTRIBUTION CODE

13. ABSTRACT *(Maximum 200 words)*

This guideline document covers the use of the subthreshold charge separation technique for analysis of ionizing radiation degradation of gate dielectrics in MOSFETs and isolation oxide degradation in parasitic FETs. The subthreshold technique is used to separate radiation induced threshold voltage shifts into voltage shifts due to oxide trapped holes and interface states. The theory and assumptions of this technique are discussed in detail. The application is discussed with respect to electrical measurements and data analysis. Limitations in the application with regard to interferences from leakage and violations of assumptions are presented. In the appendix, a proposed measurement and data analysis standard is given.

14. SUBJECT TERMS		15. NUMBER OF PAGES
Subthreshold	Total Dose	98
Oxide Trapped Charge	Interface States	16. PRICE CODE

17. SECURITY CLASSIFICATION OF REPORT	18. SECURITY CLASSIFICATION OF THIS PAGE	19. SECURITY CLASSIFICATION OF ABSTRACT	20. LIMITATION OF ABSTRACT
UNCLASSIFIED	UNCLASSIFIED	UNCLASSIFIED	SAR

CONVERSION TABLE

Conversion factors for U.S. Customary to metric (SI) units of measurement

MULTIPLY →	BY →	TO GET
TO GET ←	BY ←	DIVIDE

angstrom	1.000000 x E -10	meters (m)
atmosphere (normal)	1.01325 x E +2	kilo pascal (kPa)
bar	1.000000 x E +2	kilo pascal (kPa)
barn	1.000000 x E -28	meter^2 (m^2)
British thermal unit (thermochemical)	1.054350 x E +3	joule (J)
calorie (thermochemical)	4.184000	joule (J)
cal (thermochemical) / cm^2	4.184000 x E -2	mega joule/m^2 (MJ/m^2)
curie	3.700000 x E +1	*giga becquerel (GBq)
degree (angle)	1.745329 x E -2	radian (rad)
degree Farenheit	$t_K = (t_F + 459.67)/1.8$	degree kelvin (K)
electron volt	1.60219 x E -19	joule (J)
erg	1.000000 x E -7	joule (J)
erg/second	1.000000 x E -7	watt (W)
foot	3.048000 x E -1	meter (m)
foot-pound-force	1.355818	joule (J)
gallon (U.S. liquid)	3.785412 x E -3	meter^3 (m^3)
inch	2.540000 x E -2	meter (m)
jerk	1.000000 x E +9	joule (J)
joule/kilogram (J/kg) (radiation dose absorbed)	1.000000	Gray (Gy)
kilotons	4.183	terajoules
kip (1000 lbf)	4.448222 x E +3	newton (N)
kip/inch^2 (ksi)	6.894757 x E +3	kilo pascal (kPa)
ktap	1.000000 x E +2	newton-second/m^2 (N-s/m^2)
micron	1.000000 x E -6	meter (m)
mil	2.540000 x E -5	meter (m)
mile (international)	1.609344 x E +3	meter (m)
ounce	2.834952 x E -2	kilogram (kg)
pound-force (lbs avoirdupois)	4.448222	newton (N)
pound-force inch	1.129848 x E -1	newton-meter (N.m)
pound-force/inch	1.751268 x E +2	newton/meter (N/m)
pound-force/foot^2	4.788026 x E -2	kilo pascal (kPa)
pound-force/inch^2 (psi)	6.894757	kilo pascal (kPa)
pound-mass (lbm avoirdupois)	4.535924 x E -1	kilogram (kg)
pound-mass-foot^2 (moment of inertia)	4.214011 x E -2	kilogram-meter^2 (kg.m^2)
pound-mass/foot^3	1.601846 x E +1	kilogram/meter^3 (kg/m^3)
rad (radiation dose absorbed)	1.000000 x E -2	**Gray (Gy)
roentgen	2.579760 x E -4	coulomb/kilogram (C/kg)
shake	1.000000 x E -8	second (s)
slug	1.459390 x E +1	kilogram (kg)
torr (mm Hg, 0° C)	1.333220 x E -1	kilo pascal (kPa)

*The becquerel (Bq) is the SI unit of radioactivity; 1 Bq = 1 event/s.
**The Gray (Gy) is the SI unit of absorbed radiation.

TABLE OF CONTENTS

TABLE OF CONTENTS (Concluded)

LIST OF ILLUSTRATIONS

LIST OF ILLUSTRATIONS (Concluded)

SECTION 1

INTRODUCTION

Silicon microcircuits which use SiO_2 for the gate dielectric and/or surface passivation degrade when exposed to ionizing radiation. The degradation results from two phenomena:

1. Radiation induced trapped holes, ΔN_{OT}; and
2. Radiation induced interface states ΔN_{IT}.

The details of the creation and annihilation of these two charge components have been studied for the past 30 years since the discovery of ionization induced degradation of transistors in an early satellite. The research has involved hole-electron pair generation and recombination in SiO_2, hole transport and trapping, interface state formation mechanisms, the chemical structure of the hole trap and interface state, the energy density of the interface states, the detrapping mechanisms of trapped holes, and the annihilation mechanisms f interface states. Many models have been developed for the observed characteristics and their dependence on dose, dose rate, electric field, temperature, oxide thickness, and oxide processing details. Most of the research to characterize the radiation induced trapped hole and interface state densities has been done with a nearly ideal, one-dimensional test structure, the MOS capacitor, MOSC. The primary techniques used to study the mechanisms of ΔN_{OT} and ΔN_{IT} on capacitors involve capacitance-voltage or conductance-voltage characteristics. These measurements are made at various temperatures, sweep rates, and frequencies to characterize the trapping and detrapping of ΔN_{OT} and the energy dependence of ΔN_{IT}. Other techniques involving charge injection and gate current measurements are used to measure the spatial dependence and energy levels of the trapped holes.

Although the MOSC is an ideal structure for studying the physics of ΔN_{OT} and ΔN_{IT}, it is not a practical test structure for engineering applications such as device characterization and hardness assurance. Some of the reasons include:

1. MOSCs are not used to build microcircuits.
2. MOSCs cannot be used to study parasitics, e.g., sidewall and backchannel leakage in SOS and SOI.
3. Practical bias conditions cannot be evaluated, e.g., PN junction bias.
4. Geometrical effects cannot be evaluated, e.g., gate length and width.
5. MOSCs are usually large and hence are seldom included on microcircuit die as test structures.

It has long been recognized that the most practical test structure for characterizing the ionization response of MOS microcircuits is the MOS transistor, MOSFET, since it is the primary circuit element which determines the failure level of the microcircuit. It has also been shown that in bipolar microcircuit technologies which use recessed field oxides, the dominate failure mode (buried layer to buried layer leakage) is best characterized by a parasitic MOSFET structure. There are two principal reasons why the MOSFET has not been used extensively in the past as the test structure of choice to study and characterize ΔN_{OT} and ΔN_{IT}. First, the techniques for separating the two charge components using transistor measurements have only recently been developed. Second, the characteristics which make the transistor the more practical test structure often result in limitations which make it less ideal for studying the physics of ΔN_{OT} and ΔN_{IT}. For example, the geometric, bias and parasitic effects which are often important in understanding failure mechanisms in actual microcircuits often result in a distortion of the transistor electrical characteristics which make it difficult to separate out the ΔN_{OT} and ΔN_{IT} in the active gate oxide.

If the MOSC is the ideal structure for studying the physics of ΔN_{OT} and ΔN_{IT}, and the MOSFET is the ideal structure for studying the component degradation which results in microcircuit failure, then it is reasonable to question why charge separation needs to be performed on MOSFETs.

Since the development of MOS microcircuit technologies in the late 1960's, most analyses of microcircuit failure were based on the threshold voltage shift, ΔV_{TH},

which, in early MOS technologies, had a negative shift due to trapped holes. However, as process hardening techniques developed to reduce the hole trapping efficiency and oxides were thinned, resulting in fewer available holes per rad, the trapped hole density was no longer the only charge component which had to be considered. Several failure mechanisms relating to interface states started to become dominate such as, a) mobility degradation, and b) positive threshold voltage shifts in n-channel MOSFETs referred to as "rebound" or "super-recovery". [1] Thus, in many modern MOS microcircuit technologies which have thin oxides, or have been process hardened to reduced hole trapping, both ΔN_{OT} and ΔN_{IT} are important. Also, because ΔV_{OT}, the voltage shift resulting from ΔN_{OT}, and ΔV_{IT}, the voltage shift resulting from ΔN_{IT}, have opposite signs in n-channel devices, one can perform "hardening" by balancing the two components. However, since the buildup and decay of ΔV_{OT} and ΔV_{IT} have different time constants associated with them, the balancing of ΔV_{OT} and ΔV_{IT} only works over a limited range of dose rates and/or annealing times. Also, buildup of interface states can degrade mobility resulting in speed degradation of the microcircuit. Therefore, "total dose" response is not single valued, since the values of ΔV_{OT} and ΔV_{IT} at a given total dose may vary significantly depending on the dose rate or measurement time.[2] It is mandatory in most modern MOS technologies to separate ΔV_{OT} and ΔV_{IT} in order to evaluate the ionization hardness. A part which is hard to many megarads when tested with a ^{60}Co source at 200 rads/s, one hour after irradiation (see MIL-STD-883 method 1019), may fail at a significantly lower dose when tested at high dose rate (weapon environment) or low dose rate (space environment). The reason is that the part may have a high ΔV_{OT} and a high ΔV_{IT} at intermediate dose rates which balance to prevent failure. At the high dose rate, failure is dominated by ΔN_{OT} mechanisms, and at low dose rates failure is dominated by ΔN_{IT} mechanisms. In fact, the values of ΔV_{OT} and ΔV_{IT} could possibly be used as hardness measures for the high dose rate and low dose rate environments, respectively.

Thus, there are many practical engineering applications for charge separation in MOSFETs, among them:

1. Characterization of the hardness of a technology.

2. Evaluation of the effectiveness of process techniques to reduce ΔN_{OT} and ΔN_{IT}.

3. Monitoring the process to control ΔN_{OT} and ΔN_{IT}.

4. Qualification and hardness assurance of process lots.

For engineering applications, such as the four mentioned here, it is probably not necessary to determine the actual values of ΔN_{OT} or ΔN_{IT}, but rather the voltage components ΔV_{OT} and ΔV_{IT}. ΔV_{OT} is proportional to the "effective" trapped hole density and ΔV_{IT} is a measure of the net charge of the interface states at threshold.

There have been a number of charge extraction techniques developed for MOSFETs over the past few years. However, most of these techniques have been developed to extract $\Delta N_{IT}(\Delta V_{IT})$. Only one technique has been proposed to extract $\Delta N_{OT}(\Delta V_{OT})$.[3] The ΔN_{OT} technique is based on the assumption that the interface states are predominantly acceptors in the upper half of the SiO_2 band gap and donors in the lower half and that the net charge of the interface states is approximately zero at midgap.[4] This assumption has long been used to extract ΔN_{IT} using MOSC C-V characteristics. Several techniques have been developed to extract ΔN_{IT} from MOSFET characteristics. Among these are:

a. Subthreshold swing;[5,6]

b. Weak inversion;[7]

c. Mobility;[8]

d. Charge pumping;[9] and

e. Deep level transient spectroscopy.[10]

The weak inversion technique is used to find the value of ΔN_{IT} at a single surface potential half way between midgap and inversion. The mobility technique is based on the work of Sun and Plummer[11] who showed that the process induced oxide fixed charge, Q_{SS}, which is located within 50 $\AA$ of the SiO_2–Si interface, caused a degradation of surface mobility according to the relation

$$\mu = \frac{\mu_o}{1 + \alpha Q_{SS}},$$

where μ is the degraded mobility, μ_o the "ideal" mobility, and α an empirical coefficient. Galloway[8] used this relationship to describe the radiation induced degradation of mobility by interface states in the form

$$\mu = \frac{\mu_o}{1 + \alpha \Delta N_{IT}},$$

where μ is now the post-irradiation mobility, μ_o the pre-irradiation mobility, and α is an empirical coefficient which may vary with process. Charge pumping is a technique which can be used to measure ΔN_{IT} based on a substrate (channel) current proportional to the number of interface states charged and discharged by sweeping the surface potential. The charge pumping technique requires a separate contact to the substrate/channel and does not use conventional MOSFET I-V characteristics. The deep level transient spectroscopy (DLTS) technique has only recently been applied to MOSFETs. This technique is not practical for engineering applications because measurements must be made over a wide range of temperatures.

The subthreshold technique, which was first presented in 1984[3] and was formalized in 1986,[12] is based on standard I-V characteristics and is the only technique which combines a method for ΔV_{OT} and ΔV_{IT}. The subthreshold drain current at a fixed drain to source voltage, V_{DS}, is measured as a function of gate voltage from the leakage current (or limiting resolution of the measurement system) through inversion. In an ideal device, the drain current and gate voltage are related by $I_D \propto \exp(V_G)$. When plotted as log I_D versus V_G, the straight I-V characteristic can be extrapolated to a calculated midgap current. Comparing the pre- and post-irradiation characteristics, the midgap voltage shift, ΔV_{MG}, as well as the change in subthreshold swing (inverse slope), ΔS, can be determined. The value of ΔV_{MG} is equivalent to ΔV_{OT} and ΔS is proportional to ΔV_{IT}. The subthreshold charge separation technique has proven to be the easiest to perform and is the most widely used. However, as will be discussed in detail in this document, there are many limitations to the technique.

The purpose of this document is to provide guidance in the use of the subthreshold charge/voltage separation technique. To this end, the theory and assumptions are discussed in detail. The applications of the technique are discussed with respect to electrical measurement techniques and data analysis. Finally, the limitations

of the technique are discussed with regard to interferences from leakage, parasitics, and violation of assumptions. In the Appendix, a proposed measurement and data analysis standard is given.

SECTION 2

MOSFET SUBTHRESHOLD THEORY

MOSFET subthreshold theory refers to the electrical characteristics of the transistor in weak inversion. In weak inversion, the current in the channel is dominated by diffusion of minority carriers. This differs from strong inversion channel current which is dominated by electric field assisted majority carrier transport. The subthreshold current is used to determine the shift in threshold voltage due to trapped holes, ΔV_{OT}, and interface states, ΔV_{IT}. The accuracy of this calculation is dependent on whether assumptions used to develop the subthreshold charge separation technique are violated. The theory, together with the assumptions, predicts a near linear subthreshold swing (mV/decade) for a MOSFET. A nonlinear swing may imply a violation of an assumption or the effect of a variable not considered in the theoretical development. In this section, the MOSFET subthreshold theory is presented. In Section 3, violations of assumptions are checked to determine their theoretical effect on the subthreshold charge separation technique. Most important, their effect on the subthreshold swing and analysis.

2.1 THEORETICAL MOSFET WEAK INVERSION CHANNEL CURRENT.

In a MOSFET, the theoretical subthreshold channel current, I_o, is given by

$$I_o = \mu \left(\frac{Z}{L}\right) \left(\frac{n_i}{N}\right)^2 \frac{aC_{ox}}{2\beta^2} e^{\beta\phi_S} \left(\beta\phi_S - 1\right)^{-1/2}, \tag{1}$$

where

μ = effective mobility,
N = interface doping,
n_i = intrinsic doping concentration,

Z = channel width,
L = channel length,
β = q/kT,
ϕ_S = surface potential,
a = $\sqrt{2}\,(\varepsilon_s/L_D)\,/C_{ox}$,
ε_s = silicon dielectric constant,
L_D = debye length,
$C_{ox} = \varepsilon_{ox}/t_{ox}$,
ε_{ox} = oxide dielectric constant,
t_{ox} = oxide thickness.

and drain voltage is greater than a few kT/q.

This equation is derived using Brews' charge sheet model.[13,5] The current in this case refers to the current which flows in the channel of the device. It does not include gate and substrate leakages or any other parasitic effect. The channel current in equation (1) is a strong function of the surface potential. Gate voltage is related to the surface potential so that the $dV_G/d\ell nI_D$ can be calculated. This derivative gives the gate-voltage swing needed to reduce the current one decade, and is called the subthreshold swing. The subthreshold swing, S, is defined by

$$S = \beta^{-1}\ell n10\frac{d\beta V_G}{d\beta\phi_S}\cdot\frac{d\beta\phi_S}{d\ell nI_o}. \qquad (2)$$

Changes in the variables, which determine the channel current, can affect the subthreshold swing, if they are a function of the surface potential. Equation (1) is used to determine the midgap current in the subthreshold technique. It can also be used to determine the inversion current and thereby the inversion voltage, if the threshold voltage is not measured. Changes in any of the variables in equation (1) will change the value of the midgap and inversion currents.

To calculate the derivative in equation (2), a function relating the gate voltage to the surface potential is needed. Using depletion charge, the following equation

was constructed by Brews,[13]

$$\beta V_G = \beta\phi_S + a\left(\beta\phi_S - 1\right)^{1/2}. \tag{3}$$

Using equations (2) and (3), and assuming all coefficients are constant with surface potential, the derivative in equation (2) can be calculated and the subthreshold swing becomes

$$S = \beta^{-1}\ell n 10 \frac{\left[1 + \frac{C_D}{C_{ox}}\right]}{\left[1 - \frac{2}{a^2}\left(\frac{C_D}{C_{ox}}\right)^2\right]}, \tag{4}$$

where

C_D = channel depletion capacitance.

This is the equation on which the subthreshold charge separation technique is based. Usually the denominator in equation (4) is assumed to be 1.0 (i.e., it is assumed that a $\gg C_D/C_{ox}$).

The subthreshold swing is not theoretically constant from midgap to inversion. This is due to the depletion capacitance terms in equation (4). The depletion capacitance results from the depletion of majority carriers in the channel region and is in series with the insulator (gate) capacitance. As the surface potential is increased, the depletion region grows and the total capacitance decreases. The total capacitance continues to decrease until an inversion layer is formed and the total capacitance sharply increases. This process affects the subthreshold swing, because the depletion capacitance varies with the surface potential. The minimum total capacitance occurs between midgap and inversion, and this is also the point at which the minimum subthreshold swing occurs. The swing increases as the surface potential is increased or decreased. For a typical device, the pre-irradiation deviation from linear is small, as is shown in Figure 1.

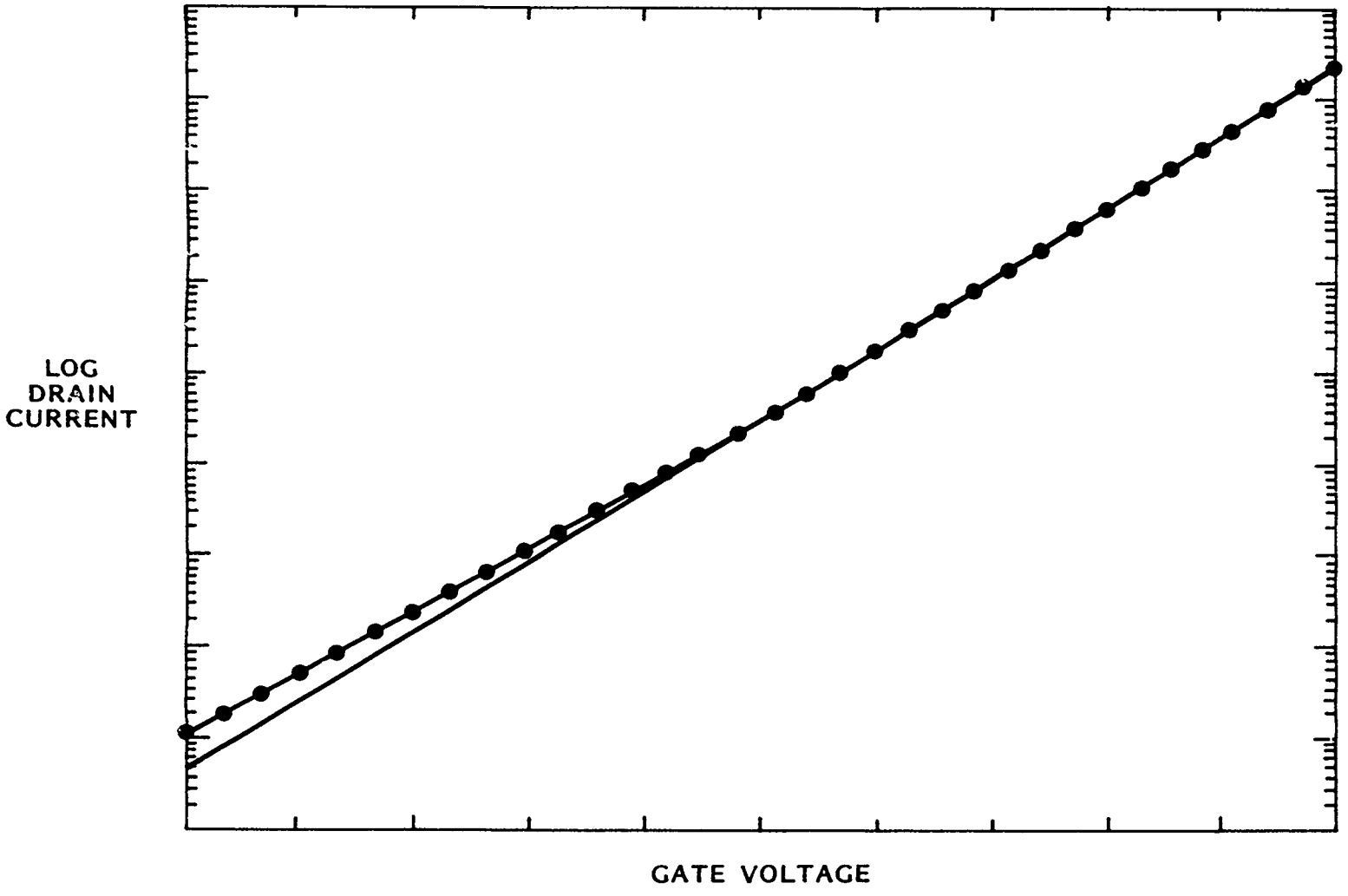

Figure 1. Difference of the theoretical subthreshold drain current from linear due to depletion capacitance.

2.2 SUBTHRESHOLD CHARGE SEPARATION TECHNIQUE.

There are two methods to separate the threshold or inversion voltage into a voltage shift due to oxide trapped holes, ΔV_{OT}, and interface states, ΔV_{IT}, using the subthreshold technique. The two methods depend on whether ΔV_{OT} or ΔV_{IT} is directly calculated from the subthreshold curve and are referred to as:

1. Midgap voltage method,
2. Subthreshold swing method.

The application of either method is dependent on whether the measured threshold voltage or the calculated inversion voltage is used.

2.2.1 Determination of ΔV_{INV} and ΔV_{TH}.

2.2.1.1 Inversion Voltage. The onset of strong inversion occurs at a gate voltage corresponding to a surface potential, ϕ_S, equal to twice the bulk fermi level, ϕ_B, where

$$\phi_S = 2\phi_B = \frac{2kT}{q} \ell n \left(\frac{N}{n_i}\right). \tag{5}$$

The gate voltage at this surface potential is referred to as the inversion voltage, V_{INV}. The channel current for strong inversion, I_{INV}, is calculated using equation (1) with $\phi_S = 2\phi_B$. V_{INV} is the gate voltage at I_{INV} which is determined by interpolating the I_D versus V_G data. I_{INV} and V_{INV} are illustrated in Figure 2. Figure 2 is a plot of log I_D versus V_G at V_D = 100 mV for a typical n-channel MOSFET. In order to calculate I_{INV}, the following parameters must be known: Z, L_{eff}, μ, t_{ox}, N, and V_D. This parameter set can be reduced if the peak transconductance, G_M, is determined from the experimental data. Since

$$G_M = \left.\frac{\Delta I_D}{\Delta V_G}\right|_{V_D} = \frac{Z\mu C_{ox} V_D}{L_{eff}}, \tag{6}$$

then

$$I_{INV} = \frac{G_M}{V_D}\frac{a}{2\beta^2}\frac{{n_i}^2}{N}\frac{e^{2\beta\phi_B}}{(2\beta\phi_B - 1)^{1/2}} \qquad V_D \gg kT/q, \tag{7}$$

where V_D is the drain voltage.

Using equation (7), the parameter set required to calculate I_{INV} is reduced to t_{ox} and N, since the remaining information can be determined from the experimental data.

The pre-irradiation value of the inversion voltage, V_{INVI}, is found from the pre-irradiation value of I_{INV} using the pre-irradiation value of G_M. However, because of the exponential dependence of I_D on V_G, a factor of 2 or 3 error in I_{INV} will only result in a small percentage change in V_{INVI}. The error will remain small if the post-irradiation value of I_{INV} is set equal to the pre-irradiation value. Therefore, the post-irradiation value of the inversion voltage, $V_{INV\gamma}$, can be determined by interpolating the post-irradiation I_D versus V_G curve. The irradiation induced inversion voltage shift, ΔV_{INV}, is determined from the following relation

$$\Delta V_{INV} = V_{INV\gamma} - V_{INVI}. \tag{8}$$

2.2.1.2 **Threshold Voltage.** The parameter most often used to characterize the radiation hardness of an MOS transistor is the threshold voltage V_{TH}. For drain voltage greater than $(V_G - V_{TH})$, the transistor is in saturation, and $I_D \propto (V_G - V_{TH})^2$. Therefore, a plot of $\sqrt{I_D}$ versus V_G should yield a straight line. If $\sqrt{I_D}$ versus V_G is extrapolated to $I_D = 0$, the V_G intercept will be V_{TH}. If the drain voltage is less than $(V_G - V_{TH})$, the transistor is in the linear region, and a plot of I_D versus V_G should yield a straight line. V_{TH} is found by extrapolating I_D versus V_G to $I_D = 0$. ΔV_{TH} is given by

$$\Delta V_{TH} = V_{TH\gamma} - V_{THI}, \tag{9}$$

where $V_{TH\gamma}$ and V_{THI} are the post- and pre-irradiation threshold voltages, respectively.

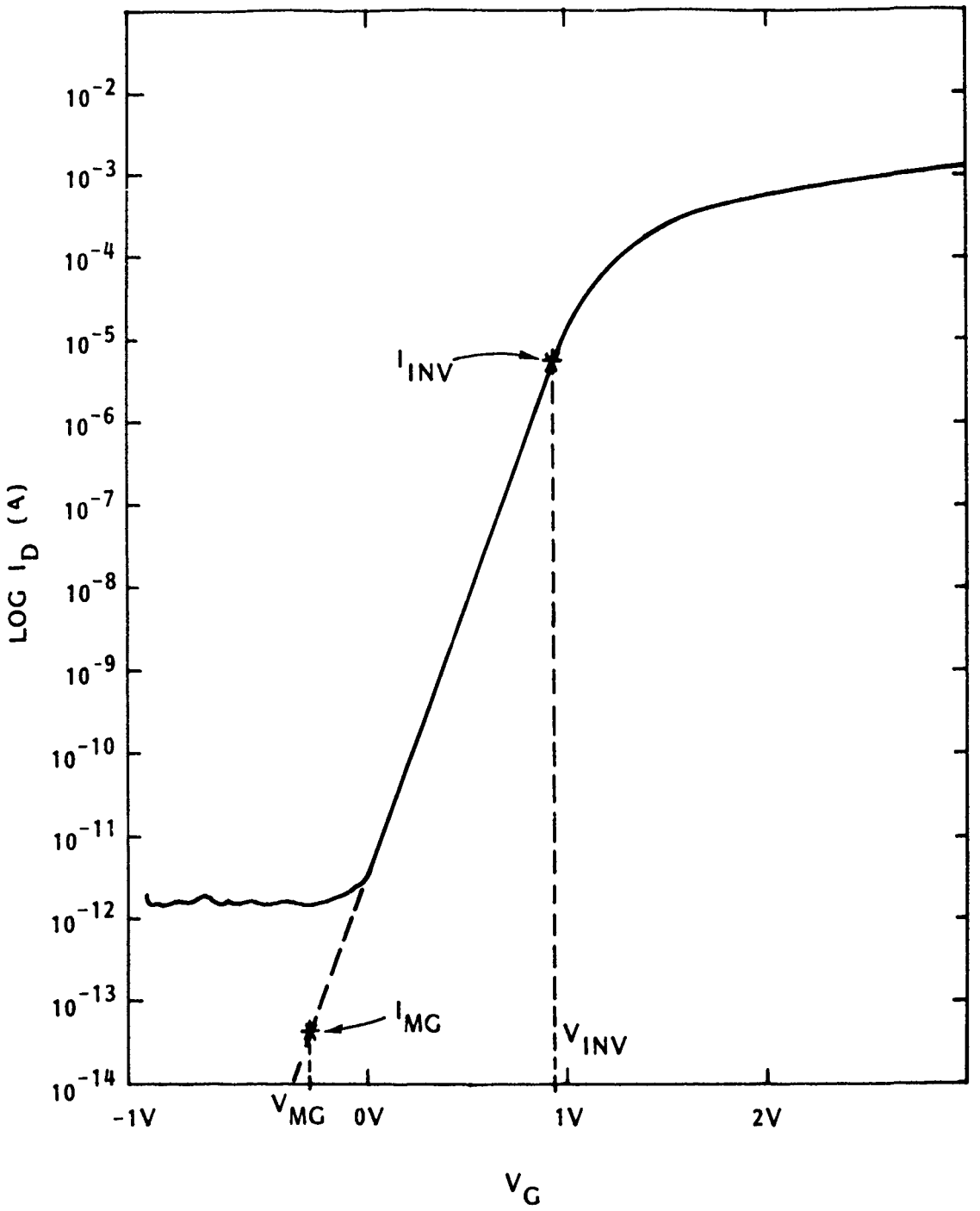

Figure 2. Typical n-channel plot of log I_D versus V_G showing extrapolation to a calculated midgap current.

2.2.2 Midgap Voltage Method.

The midgap voltage method of the subthreshold charge separation technique is based on two calculations: 1) the radiation induced voltage shift from oxide trapped charge, ΔV_{OT}, using the change in midgap voltage, ΔV_{MG}, and 2) the radiation induced voltage shift from interface states, ΔV_{IT}, using ΔV_{MG} and the change in the threshold voltage, ΔV_{TH}, or the inversion voltage, ΔV_{INV}.

2.2.2.1 $\underline{\Delta V_{OT}}$. The value of ΔV_{OT} is obtained from ΔV_{MG} assuming the following relation:

$$\Delta V_{OT} = \Delta V_{MG} = \frac{q\Delta N_{OT}}{C_{ox}}, \tag{10}$$

where $C_{ox} = \varepsilon_{ox}/t_{ox} = 3.45 \times 10^{19}/t_{ox}\ F/cm$ for SiO_2, and ΔN_{OT} is the radiation induced trapped hole density. Equation (10) is based on the following assumptions:

a. The trapped hole density is a uniform sheet charge at the interface; and

b. The net charge of the interface states at midgap is zero.[4]

For relatively thin gate oxides (200–1000 $\AA$), the spatial distribution of the trapped holes has been determined using a number of indirect techniques. Except for a narrow region within 20–50 $\AA$ of the interface where trapped holes are quickly compensated or removed by electrons tunneling from the silicon, the trapped holes are located within 50–150 $\AA$ of the oxide.[14] The actual spatial dependence of the trapped hole density within this region is not well known but is probably best represented by a double exponential peaking around 30–50 $\AA$. For some oxides, e.g., commercial soft gate oxides[14] and thick field oxides,[15] the holes may be nearly uniformly trapped in the oxide bulk. In the case of the uniform trapping, the midgap shift is only 1/2 of the value for a sheet charge at the interface and hence,

$$\Delta V_{MG} = \frac{q\Delta N_{OT}}{2C_{ox}}. \tag{11}$$

In the application of the subthreshold charge separation technique, the radiation induced interface states are assumed to be primarily acceptors in the upper half of the band gap and donors in the lower half. Near midgap, the net charge of the interface states is approximately zero.[4] If the net charge of the interface states at midgap is zero, then the change in midgap voltage is a result of the net oxide trapped charge which is assumed to be holes.

The midgap voltage usually cannot be measured directly because the channel current at midgap is usually smaller than the leakage current and/or too small to measure with conventional picoammeters or electrometers. Therefore, an extrapolation technique is used to determine the midgap voltage from channel current, I_o, versus gate voltage, V_G, in subthreshold. The channel current in subthreshold (weak inversion) is given in equation (1).

The channel current at midgap, I_{MG}, can be found by substituting the midgap value of surface potential, ϕ_B, where

$$\phi_S = \phi_B = \frac{kT}{q} \ell n \left(\frac{N}{n_i} \right), \tag{12}$$

into equation (1). The midgap voltage, V_{MG} is the gate voltage at I_{MG} found by extrapolating the measured subthreshold characteristic. Figure 2 is a plot of log I_D versus V_G at $V_D = 100$ mV for a typical n-channel MOSFET showing the extrapolation of I_D to I_{MG}. Using equation (1), I_{MG} is calculated similar to I_{INV} with $\phi_S = \phi_B$.

The pre-irradiation value of midgap voltage, V_{MGI}, is found from the pre-irradiation value of I_{MG} using the pre-irradiation value of G_M. The value of I_{MG} calculated in this manner will be somewhat low, since the mobility in subthreshold may not be constant and may increase as the surface potential is lowered. Therefore, the post-irradiation value of midgap voltage, V_{MG_7}, can be determined by extrapolating the post-irradiation I_D versus V_G curve to I_{MGI}. ΔV_{MG} is determined from the following relation

$$\Delta V_{MG} = V_{MG_7} - V_{MGI}. \tag{13}$$

2.2.2.2 $\underline{\Delta V_{IT}}$. The radiation induced voltage shift due to charged interface states is assumed to be that portion of the inversion voltage shift or threshold voltage shift which is not due to the trapped holes. The use of inversion voltage is more mathematically correct since it is the value of gate voltage for a specified value of surface potential. However, the use of threshold voltage, which is an empirical value, is more practical since it is the parameter specified on data sheets and generally used to measure radiation performance.

The inversion voltage change due to irradiation, ΔV_{INV}, is a result of the voltage shift due to oxide trapped charge, ΔV_{OT}, and the voltage shift due to the charged interface states, ΔV_{IT}. In n-channel devices, the value of ΔV_{IT} is positive due to the predominance of acceptors, and in p-channel devices, ΔV_{IT} is negative due to the predominance of donors. Using the midgap voltage method, the value of ΔV_{IT} is found from the following relation:

$$\Delta V_{IT} = \Delta V_{INV} - \Delta V_{OT}. \tag{14}$$

As with the midgap voltage shift, the pre-irradiation and post-irradiation values of I_{INV} are calculated using the pre-irradiation value of transconductance.

Using ΔV_{TH} instead of ΔV_{INV}, ΔV_{IT} is determined from the following relation:

$$\Delta V_{IT} = \Delta V_{TH} - \Delta V_{OT}. \tag{15}$$

2.2.3 Subthreshold Swing Method.

The subthreshold swing method of the charge separation technique is based on two calculations: 1) the radiation induced voltage shift due to interface states, ΔV_{IT}, using the change subthreshold swing, ΔS, and 2) the radiation induced shift from oxide trapped holes, ΔV_{OT}, using ΔV_{IT}, and the change in threshold voltage, ΔV_{TH}, or the inversion voltage, ΔV_{INV}.

2.2.3.1 $\underline{\Delta V_{IT}}$. Assuming $a \gg C_D/C_{ox}$, equation (4) can be rewritten, which gives

$$S = \frac{kT}{q}\ell n10\,(1 + C_D/C_{ox})\,. \tag{16}$$

If the pre-irradiation value of the subthreshold swing, S_I, is defined by equation (16), the post-irradiation subthreshold swing, S_γ, is defined by

$$S_\gamma = \frac{kT}{q}\ell n10\left[1 + \frac{C_D + C_{IT}}{C_{ox}}\right]. \tag{17}$$

The difference between the pre- and post-irradiation subthreshold swings, ΔS, is

$$\Delta S = S_\gamma - S_I = \frac{kT}{q}\ell n10\frac{C_{IT}}{C_{ox}}. \tag{18}$$

If the interface states are uniform between midgap and inversion, the interface state capacitance, C_{IT}, causes the voltage shift, ΔV_{IT}, which is equivalent to

$$\Delta V_{IT} = C_{IT}/C_{ox}\phi_B \tag{19}$$

Using equations (18) and (19), the value of ΔV_{IT} is obtained from ΔS where

$$\Delta V_{IT} = \frac{q\phi_B}{kT\ell n10}\Delta S. \tag{20}$$

Equation (20) is based on the following assumptions:

1. No lateral nonuniformities (LNUs) of trapped holes in the oxide.
2. The net charge of interface states at midgap is zero and are uniform between midgap and inversion.[4]
3. $a \gg C_D/C_{ox}$, and $a \gg (C_D + C_{IT})/C_{ox}$.

The assumption that $a \gg (C_D + C_{IT})/C_{ox}$ is a fairly stringent restraint. As the number of interface states increase, C_{IT} also increases. This assumption essentially

limits the application of this method. At high total dose levels, this assumption should be checked.

Similar to the midgap voltage method, the voltage shift due to oxide trapped holes, ΔV_{OT}, is calculated using the shift in threshold or inversion voltage from the relation

$$\Delta V_{OT} = \Delta V_{TH}\left(\Delta V_{INV}\right) - \Delta V_{IT}. \tag{21}$$

2.3 ΔN_{IT}.

The separation of ΔV_{INV} or ΔV_{TH} into ΔV_{OT} and ΔV_{IT} is a very useful engineering tool for the evaluation of radiation hardening techniques to determine the relative amounts of hole trapping and interface state generation. However, although a reasonable estimate of ΔN_{OT} can be obtained from equation (10), a reasonable estimate of ΔN_{IT} is not necessarily obtained from a similar relation for ΔV_{IT}. The value of ΔN_{IT} should be determined using the subthreshold swing, S, as described by equation (4).

If there are a significant number of interface states, the capacitance associated with these states, C_{IT}, is in parallel with C_D. This effects the value of the subthreshold swing, S, and equation (4) becomes

$$S_\gamma = \frac{kT}{q}\ell n10\left[1+\frac{C_D+C_{IT}}{C_{ox}}\right]\Big/\left[1-\frac{2}{a^2}\left(\frac{C_D+C_{IT}}{C_{ox}}\right)^2\right]. \tag{22}$$

Assuming that the pre-irradiation value of interface state density is small (e.g., $\leq 10^{10}$ cm^{-2}), the irradiation induced change in subthreshold swing is given by

$$\Delta S = S_\gamma - S_I = \frac{kT}{q}\ell n10\left[\frac{\left[1+\frac{C_D+C_{IT}}{C_{ox}}\right]}{\left[1-\frac{2}{a^2}\left(\frac{C_D+C_{IT}}{C_{ox}}\right)^2\right]} - \frac{\left[1+\frac{C_D}{C_{ox}}\right]}{\left[1-\frac{2}{a^2}\left(\frac{C_D}{C_{ox}}\right)^2\right]}\right] \tag{23}$$

where S_I is determined using equation (4). From the ratio of the post-irradiation to pre-irradiation swing, a value of C_{IT} can be calculated in terms of S_γ, S_I, C_D, a and C_{ox} as follows.

$$C_{IT} = \left(\frac{H - \left\{ H + 4\frac{S_\gamma}{S_I}\left(1+\frac{C_D}{C_{ox}}\right)\frac{2}{a^2}\left[\frac{S_\gamma}{S_I}\left(1+\frac{C_D}{C_{ox}}\right) - H\right]\right\}^{1/2}}{-2\frac{S_\gamma}{S_I}\left(1+\frac{C_D}{C_{ox}}\right)\frac{2}{a^2}} \right) C_{ox} - C_D, \qquad (24)$$

where

$$H = 1 - \frac{2}{a^2}\left(\frac{C_D}{C_{ox}}\right)^2.$$

The depletion capacitance can be determined from the pre-irradiation swing as follows

$$C_D = \left(\frac{1 - \left\{ 1 + \frac{8}{a^2} S_I \frac{\beta}{\ell n 10}\left[S_I \frac{\beta}{\ell n 10} - 1\right]\right\}^{1/2}}{-S_I \frac{4}{a^2}\frac{\beta}{\ell n 10}} \right) C_{ox}. \qquad (25)$$

The depletion capacitance defined by equation (25) includes the effects of process induced interface states. Using the pre- and post-irradiation subthreshold curves, a plot of the energy density of interface states, D_{IT}, versus ϕ_S can be determined in a manner similar to the Terman technique[16] for MOS capacitor C-V curves. If the values of S_γ and S_I are determined at several values of I_D between I_{MG} and I_{INV}, the value of D_{IT} at each I_D can be calculated using equations (24) and (25), and the relation $D_{IT} = C_{IT}/q$. The total number of interface states between midgap and inversion is found by integrating D_{IT} over energy as follows.

$$\Delta N_{IT} = \int_{\phi_B}^{2\phi_B} D_{IT} d\phi. \qquad (26)$$

If D_{IT} is constant between $\phi_S = \phi_B$ and $2\phi_B$, then

$$\Delta N_{IT} = \frac{C_{IT}}{q}\phi_B. \qquad (27)$$

Assuming, a) both the pre-irradiation and post-irradiation subthreshold channel current are exponentially dependent on V_G, b) the irradiation induced interface state

density is constant between midgap and inversion, and c) "a" is large compared to C_D/C_{ox}, then ΔN_{IT} can be found directly from ΔS or ΔV_{IT}.

$$\Delta N_{IT} = \frac{C_{ox}\Delta V_{IT}}{q} = \frac{\Delta S C_{ox}\phi_B}{kT\ell n10}, \tag{28}$$

where ΔV_{IT} is determined from equation (14) using ΔV_{INV}.

SECTION 3

DISCUSSION OF VARIABLES AND ASSUMPTIONS IN THE SUBTHRESHOLD CHARGE SEPARATION TECHNIQUE

Analysis of a MOSFET that has a near linear subthreshold swing using the subthreshold charge separation technique is well defined. The subthreshold swing is extrapolated to find the midgap voltage. The extrapolation is necessary because the midgap current is below the leakage of the device and/or the instrumentation is not capable of measuring such low current levels. When a device exhibits a nonlinear subthreshold swing, one must choose what part of the curve to extrapolate. In some cases, the choice can yield widely different midgap voltages, which affects the trapped hole and interface state calculations. The correct choice depends on the purpose of the analysis and on the robustness of the subthreshold charge separation technique. There are inherent assumptions in the theoretical development, and violations of these assumptions may or may not greatly affect the analysis results. To analyze nonlinear characteristics, the analyst must hypothesize possible causes and determine how the subthreshold technique is affected. Combining these hypotheses with the purpose of the experimentation, the analyst must determine the portion of the curve to extrapolate.

3.1 MOBILITY.

Mobility is an important parameter in equation (1). Two mobility regions can be defined in a MOSFET:

1. The mobility which occurs in strong inversion (measured via the transconductance); and
2. The mobility in weak inversion or subthreshold.

The strong inversion mobility is greatly affected by the surface of the silicon silicon-dioxide interface, since the inversion channel is often less than 300 $\mathring{A}$. In the inversion region, the vertical electric field is much greater than the transverse electric field. This pulls the carriers to the interface, lowering mobility due to the roughness (deviation from the ideal plane) of the silicon/silicon dioxide interface. The rougher the interface the lower the mobility. In the subthreshold, the electric field is smaller, and the interface roughness has less effect on the mobility. Thus, as the surface potential is lowered from strong to weak inversion, the interface roughness has less effect and the mobility increases. The mobility in equation (1) is the weak inversion mobility and can be substantially different than the strong inversion mobility determined from transconductance.

Bulk mobility in silicon is a function of total impurity concentration (the number of charged impurity atoms) and not net impurity concentration, which determines the carrier concentrations. When both N- and P-type impurities exist in silicon, acceptors receive electrons from the donors and all impurity atoms are charged (assuming total ionization). Thus, in theory, the weak inversion mobility can be no larger than the bulk mobility.

The value used for mobility affects the results of the subthreshold charge separation technique. The value of mobility determines midgap and inversion currents and hence the midgap and inversion voltages. Since the log of the channel current is linear with gate voltage, errors in the mobility appear as the log of the error on midgap and inversion voltages, unless irregularities exist in the subthreshold swing. Also, since the trapped hole and interface state voltage shifts are calculated from the difference between the pre- and post-irradiation midgap and inversion voltages, the effect of an error in mobility is further decreased. For MOSFETs with near-linear subthreshold characteristics, the technique is robust to the actual value used. If a measured threshold voltage is used instead of the theoretical inversion voltage, the error from an incorrect mobility would be larger, since only the midgap voltage is affected by the choice of the mobility. Irregularities in the subthreshold swing could enhance these errors.

The charge separation subthreshold technique assumes that the mobility is constant from midgap to inversion,

$$\frac{d\ell n\mu}{d\beta\phi_S} = 0. \tag{29}$$

If this derivative is nonzero, the subthreshold swing would be affected. For a nonzero mobility derivative, equation (4) would become

$$S = \beta^{-1}\ell n10\left(1+\frac{C_D}{C_{ox}}\right)\Big/\left[1-\frac{2}{a^2}\left(\frac{C_D}{C_{ox}}\right)^2-\frac{d\ell n\mu}{d\beta\phi_S}\right]. \tag{30}$$

If the mobility increases as surface potential is lowered, the subthreshold swing would increase; and if mobility decreases, the subthreshold swing would decrease. Fast changes in mobility over short ranges in surface potential can cause distortions in the subthreshold swing. For example, if the mobility increases from a fixed value to another over a given surface potential, then the subthreshold swing will increase over that range of surface potential. The subthreshold swing will be near identical outside that range as shown in Figure 3.

Channel mobility as a function of surface potential has been studied. Measurements of mobility have not been done for surface potentials much below inversion. The effect of surface potential and radiation induced trapped holes and interface states on channel mobility has been suggested.[17] Figure 4 shows a possible scenario for a typical unirradiated device. Little change is expected to occur in the subthreshold region. It has been generally accepted that ionizing radiation-induced interface states and trapped charges (holes) within 50 $\AA$ of the surface degrade mobility.[11] Interface states act as charged scattering centers and degrade mobility similar to impurity doping. Nonuniformity of interface states and/or trapped holes can create further degradation in the mobility by causing minority-carrier fluctuations, which have a large effect near inversion. For few trapped charges, the mobility is expected to decrease with surface potential above inversion, but for many trapped charges, it can increase with surface potential because of the decreasing effect of minority carrier fluctuations. Figure 5 shows possible effects of the radiation induced trapped charges. The curves of interest are the ones which show mobility increasing as the surface potential approaches

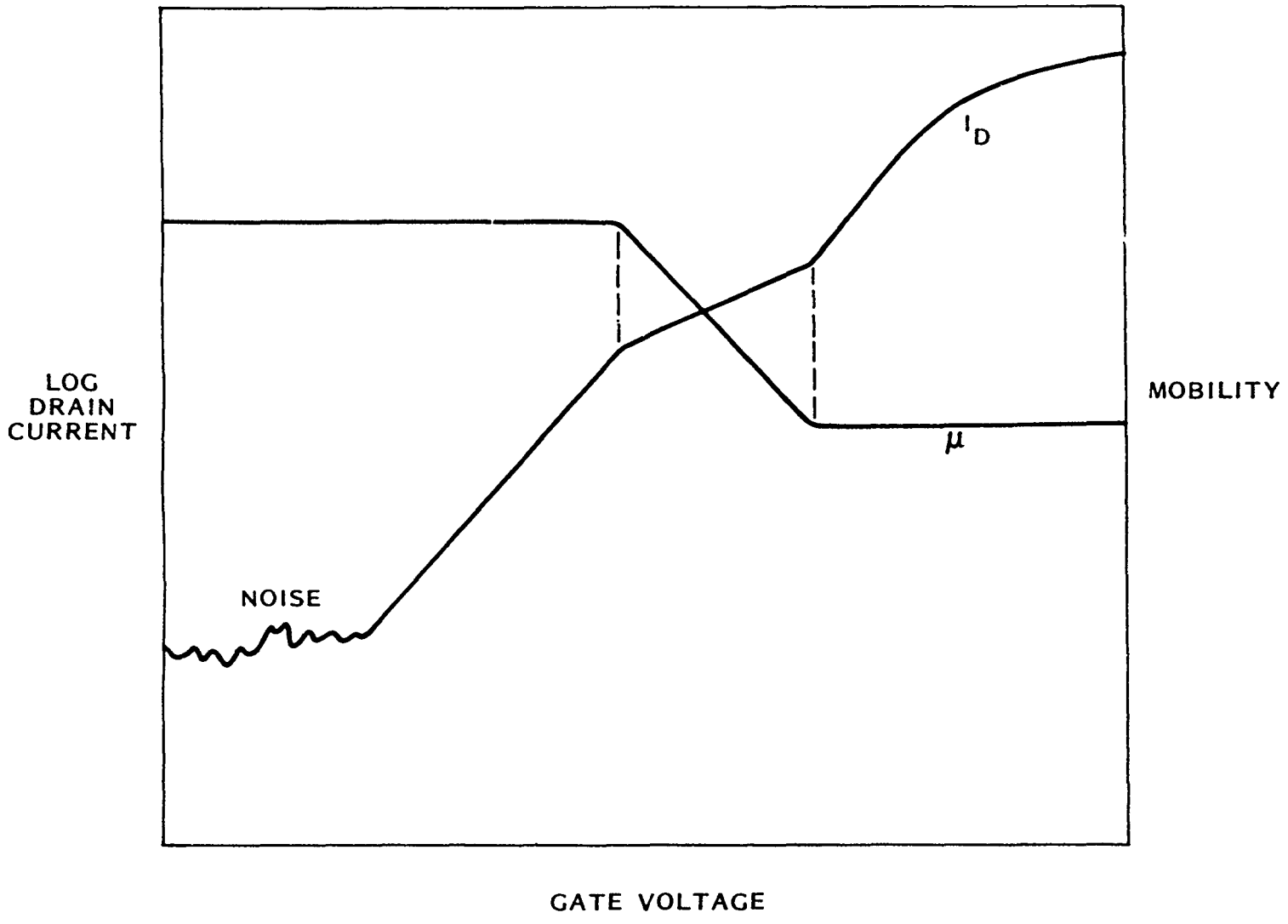

Figure 3. Effect of varying mobility on MOSFET subthreshold curve.

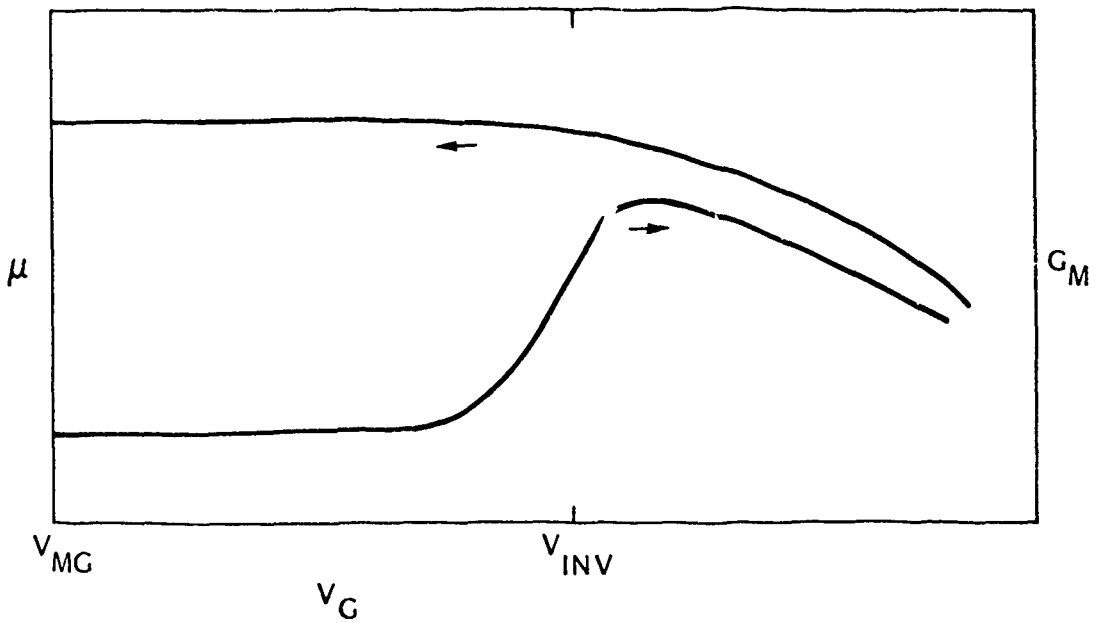

Figure 4. Typical effect of surface potential on mobility in a MOSFET.

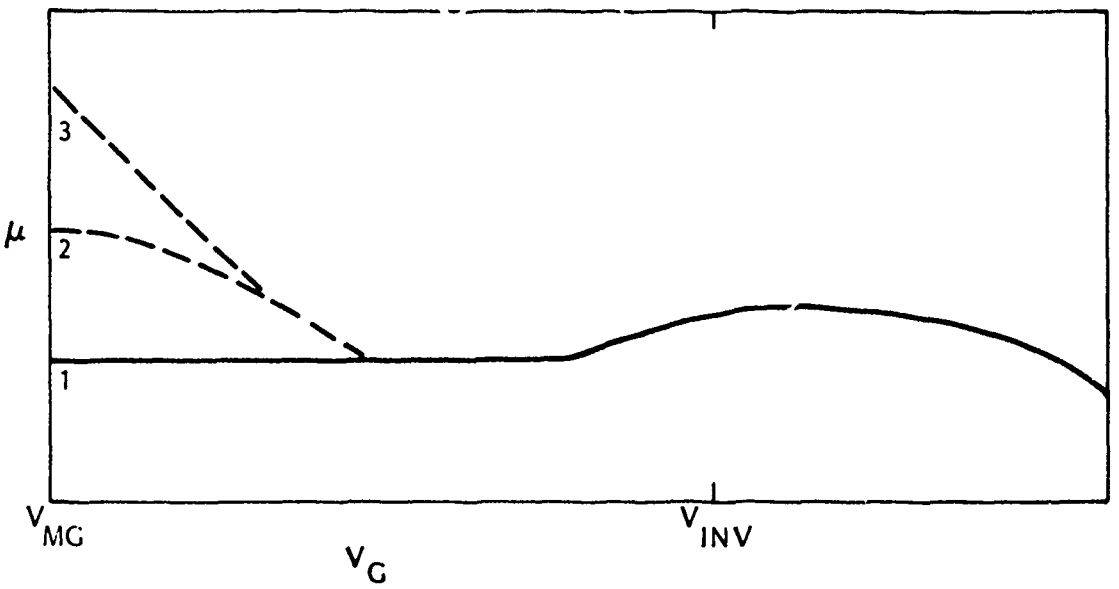

Figure 5. Possible effect of trapped charges on mobility for an irradiated MOSFET.

midgap. The hypothesis for this occurrence relies on the assumption that most interface states have neutral charge at midgap. This implies the post-irradiation mobility near midgap should improve toward the pre-irradiation condition. Since studies have shown post-irradiation mobility is degraded in the subthreshold,[17] the subsequent increase seems possible, due to the decrease in charged interface states. The question is how rapidly does the mobility increase as the surface potential approaches midgap. The increase in mobility near inversion is caused by a decreased effect from minority fluctuations.

If the mobility follows curve 3 in Figure 5, the effect on the subthreshold swing would be noticeable. At some point on the subthreshold curve, as the surface potential approached midgap, the swing would increase. This could cause a second swing or increasing swing condition as is shown in Figure 6. The lower portion of the curve has a larger voltage swing per decade. In this case, it would be caused by a changing mobility and not additional interface states in the bandgap. Extrapolation of measured data to find the midgap voltage requires judgement. The subthreshold curve will not continue at the larger swing, when the mobility is near the maximum value. Extrapolating from the top or bottom of the curve may not yield the correct midgap voltage. An example is given in Figure 7 for the effect of the increasing mobility as shown in Figure 6 on the subthreshold curve. To analyze this data using the subthreshold technique, one must decide from which part of the curve to do the linear extrapolation. Since the subthreshold technique assumes that mobility is constant and uses equation (4), the first swing (top part of the curve in Figure 7) should be used. This will give the voltage shifts caused by the interface states and trapped holes in the oxide. If the second swing is used, the technique will give the voltage shifts caused by the number of interface states and trapped holes necessary to produce the dashed line from midgap to inversion, in Figure 8. Effectively, this procedure is attempting to equate a number of interface states and trapped holes to produce the combined trapped charge and mobility effect on the subthreshold swing.

Assuming a nonconstant mobility, the choice of which part of the curve to use in Figure 7 to extrapolate depends on the purpose of the analysis. To find the correct number of trapped holes and interface states in the gate oxide, the top part

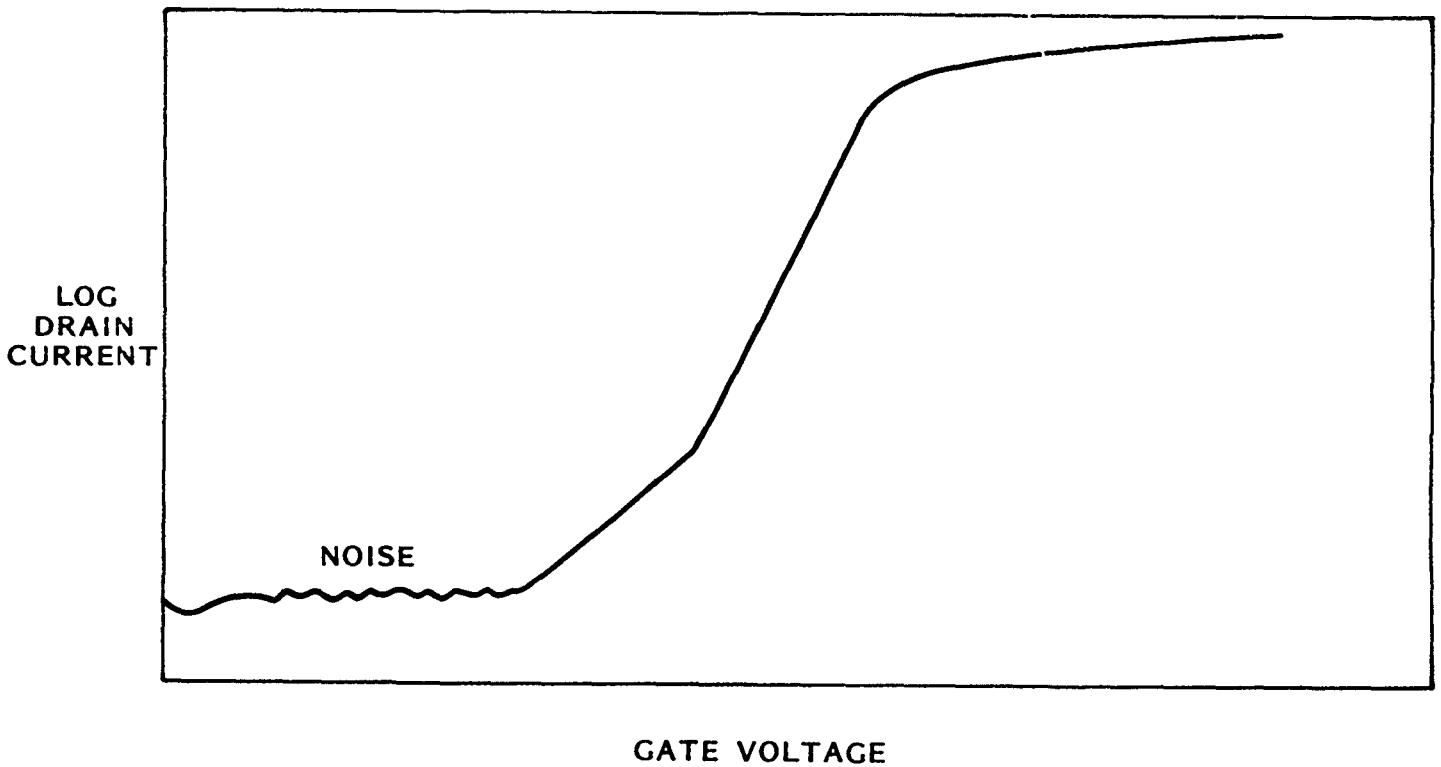

Figure 6. Effect of increasing mobility near midgap on the MOSFET subthreshold curve.

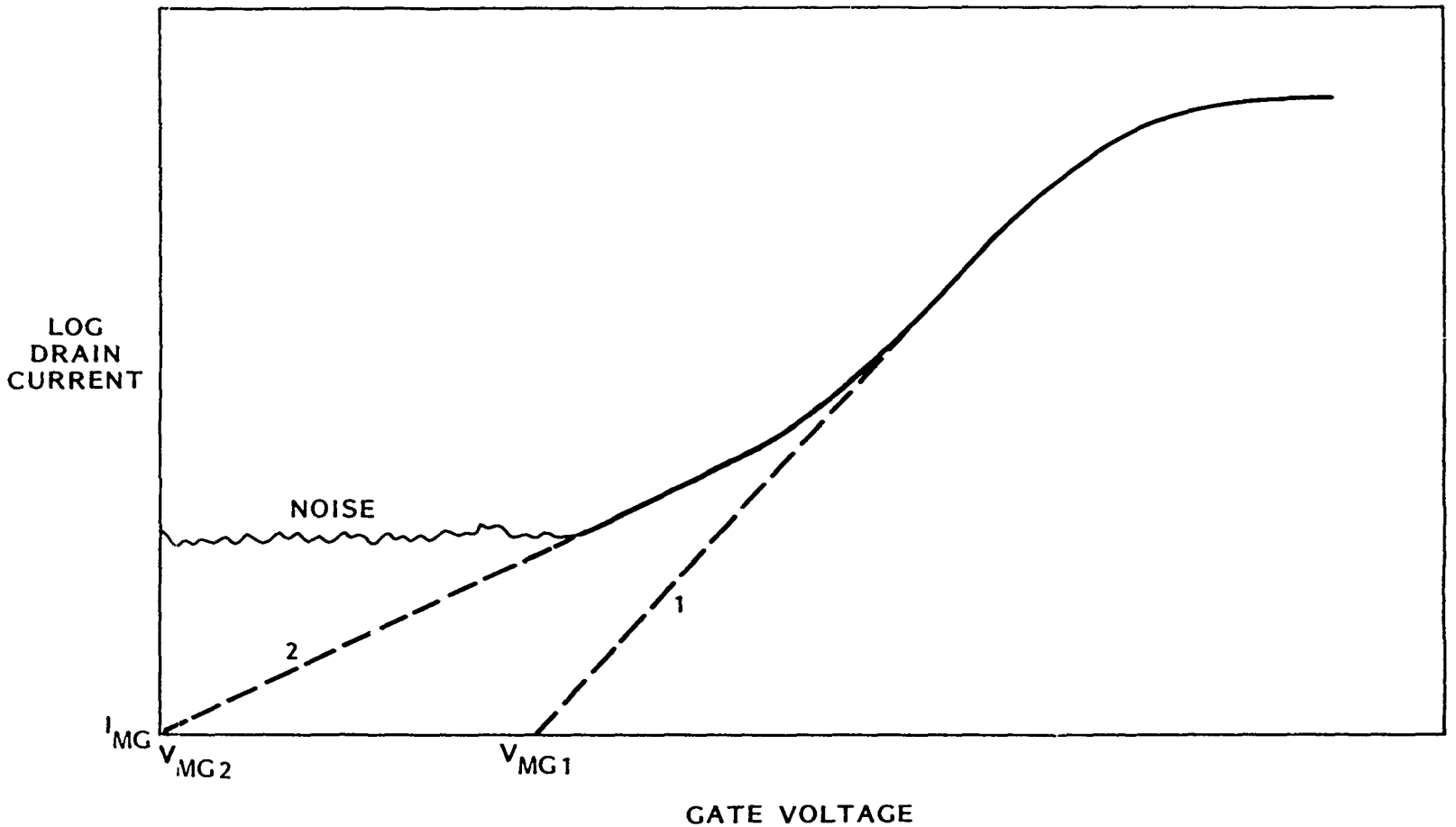

Figure 7. Effect of increasing mobility near midgap on the extrapolation of the subthreshold curve.

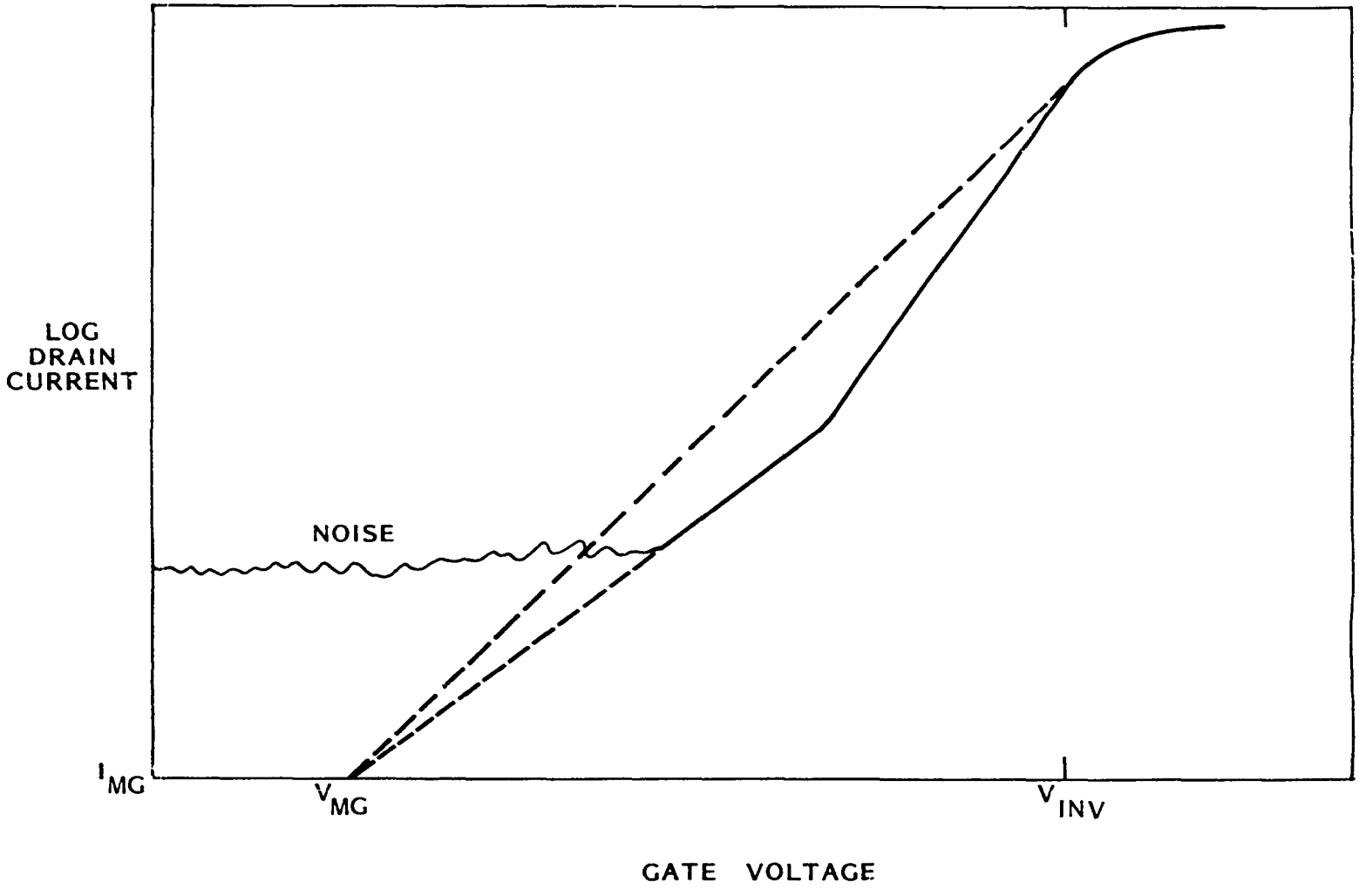

Figure 8. Voltage shifts determined from second slope are identical to the dashed line from midgap to inversion.

of the curve should be used. Extrapolating the lower part of the curve would give a conservative engineering approximation for the radiation hardness of the device, based on ΔV_{OT} and ΔV_{IT}, i.e., large numbers for both ΔV_{OT} and ΔV_{IT}. The engineering approximated total dose degraded I-V characteristic of the device would be equivalent to the dashed line from midgap to inversion in Figure 8.

3.2 CHANNEL DOPING.

Present processing methods usually will yield nonuniform doping in MOSFET channel regions. Vertical nonuniform doping occurs in MOSFETs due to the threshold adjust implant. This implant can increase the subthreshold swing depending on the depth of the implant, but it will not cause irregularities in the swing. The initial increase in the swing does not affect the subthreshold charge separation technique because of the comparison of pre- to post-irradiation curves.

MOSFETs which have nonuniform doping in the lateral direction under the gate cause a bending of the conduction and valence bands with respect to the fermi level. As a result, the entire silicon channel will not be at the same potential. When the source end of the channel is at midgap, the remainder of the channel will be above midgap. It is necessary to determine an effective channel doping to use in equation (1). Assuming the device does not turn on until the entire channel is inverted, the effective channel doping would be the larger value near the source.

3.3 LATERAL NONUNIFORMITIES (LNUs).

In recent years, LNUs have been identified as a cause for anomalous results from the application of the subthreshold charge separation technique.[18,19] LNUs appear to cause a stretchout of the subthreshold swing similar to the stretchout caused by interface states. Consequently, the voltage shift due to interface states would be overestimated and would result in an incorrect radiation characterization.

LNUs refer to lateral nonuniformities of trapped holes in the gate oxide. The surface potential at the silicon/silicon dioxide interface is directly effected by the LNUs. Irregularities of surface potential across the MOSFET channel can cause preferred current paths, so at a given surface potential the channel is not conducting current uniformly. The effect of LNUs on a MOSFET channel might be simulated as many parallel transistors all with different threshold voltages but identical subthreshold swings.[19] When the individual curves are combined, the resulting subthreshold swing is larger. The greater the spread in the individual threshold voltages, the greater the increase in the subthreshold swing.

An LNU caused increase in the subthreshold swing is interpreted as an increase in the number of interface states by the subthreshold charge separation technique. This false indication of interface states is the most serious effect of LNUs and can render the subthreshold charge separation technique as an inappropriate analysis tool. Lateral nonuniformities of trapped holes violates an assumption of the subthreshold charge separation technique that the trapped holes are uniform throughout the oxide over the channel.

It appears[19] that the creation of LNUs are radiation bias, dose rate, and energy dependent. Low energy high dose rate radiation pulses such as from an x-ray source seem to produce greater LNU effects. Also, the effects of LNUs appear to anneal at room temperature in relatively short times (less than an hour),[19] but are more stable at cryogenic temperatures.[18] Annealing of LNUs would reduce the subthreshold swing and give the appearance of interface state annealing.

LNUs in an irradiated MOSFET could possibly be identified by apparent annealing of interface states (reduction of subthreshold swing) at room temperature at early times after irradiation. The actual number of interface states in the presence of LNUs can be estimated using the subthreshold technique. If LNUs anneal at room temperature, one can assume that the LNUs have annealed after the subthreshold swing has stabilized. The value of the number of interface states calculated using the stable subthreshold swing could be used to bound the true value at earlier times. Assuming interface states are relatively stable at room temperature, this value of

the number of interface states would represent a worst case value for all times after irradiation prior to this measurement.

3.4 INTERFACE AND TRAPPED CHARGE ASSUMPTIONS.

Separation of radiation induced threshold voltage shifts into ΔV_{OT} and ΔV_{IT} using the subthreshold charge separation technique is sensitive to the assumptions about the oxide trapped charge and interface states. The subthreshold technique assumes that the interface states are amphoteric.[4] Only acceptor states are above midgap and donors are below midgap. This provides the basis for assuming that all interface traps are neutral at the midgap potential, V_{MG}. Assuming that only holes are trapped in the oxide, the midgap voltage shift, ΔV_{MG}, is representative of the quantity of trapped holes in the oxide.

Research has been performed which proposes the trapping of electrons in the oxide[20] or at the interface[21] in hardened oxides. Neither of these situations would cause non-linear subthreshold characteristics to occur. The trapped electrons would simply have a cancelling effect on the oxide trapped holes. In this case, the midgap voltage shift would represent the difference between the trapped holes and electrons and still provide a good engineering tool for judging radiation hardness.

Violation of the assumption that interface states are amphoteric would cause a non-neutral interface charge at midgap, but would not affect the linearity of the subthreshold characteristics. Research has been performed showing interface states are amphoteric[4,22] and nonamphoteric.[23] In n-channel devices, donors above midgap and in p-channel devices, acceptors below midgap will result in an overestimation by the subthreshold technique of the number of trapped holes and an underestimation of the number of interface states by the number of nonamphoteric interface states.

3.5 PARASITIC EFFECTS.

Nonideal subthreshold characteristics can be caused by parasitic effects. These effects will cause aberrations from the theoretical linear subthreshold. Parasitic effects can include:

1. Junction leakage, drain to substrate, and gate leakage to the source and/or drain.
2. Edge and parallel parasitic transistors.
3. Backchannel and edge leakage, and kink effect in a SOS or SOI MOSFET.

3.5.1 Junction Leakage.

Leakage currents mask the actual channel subthreshold current below the leakage current level and are similar to instrumentation measurement noise levels in the application of the subthreshold charge separation technique. Only the part of the curve which is above the leakage is used for the extrapolation to midgap. As with leakage current, other parasitic effects will not distort the subthreshold until the parasitic current becomes near equal to greater than the MOSFET channel current. Parasitic effects are not related to the hardness of the gate oxide to radiation-induced trapped holes and interface states, which the subthreshold charge separation technique calculates. Parasitic effects, such as leakage, may be related to the radiation hardness of the device when considered in conjunction with the circuit function.

Leakage currents are easily distinguished from the channel subthreshold current. Subthreshold analysis of this data has always been done using the data above the leakage. Data with other parasitic effects should be treated similarly. The difficulty is in identifying a parasitic effect. Any device which exhibits a subthreshold curve with significant non-linear distortions could have a parasitic effect. Applying the subthreshold charge separation technique to a portion of the curve, which contains a parasitic effect, would give misleading values of ΔN_{OT} and ΔN_{IT}. Even the voltage shifts, ΔV_{OT} and ΔV_{IT}, could be misleading, since these values imply the voltage

shifts are attributed to interface states and trapped holes in the gate oxide. Again, this reduces to using the subthreshold charge separation technique to determine the radiation hardness of the oxide, or the midgap and inversion voltage shifts due to all the effects of radiation on the device.

3.5.2 Edge and Parallel Parasitic Transistor Effects.

Edge and parallel parasitic transistor effects may cause distortion in the subthreshold curve, similar to what has been observed in power HEXFETs. Figure 9 shows an unirradiated power HEXFET, which has a bench in the subthreshold. This bench has been observed in unirradiated devices from different manufacturers. As the total dose level is increased for these devices, the pre-irradiation bench disappears, probably due to the dominance of the radiation effects. The power HEXFET may contain 10,000 or more individual MOSFETs. Nonuniformity of interface channel doping across all individual devices is possible. To determine the effect of having a few MOSFETS with different channel interface doping, a theoretical subthreshold curve was generated for a hypothetical power HEXFET. The model was run for 100 MOSFETS with a channel interface doping of 1.0×10^{14} cm^{-3}, the remaining 9,900 had an interface doping of 1.0×10^{16} cm^{-3}. This model gave a theoretical subthreshold curve shown in Figure 10. The upper part of the curve is identical to the subthreshold swing expected for the bulk of the devices. The lower part of the curve is dominated by the 100 devices with lower interface doping. Below 100 pA, the current is primarily through the 100 devices or 1.0 percent of the entire HEXFET. The bench is the transition region between the two sets of MOSFETs. The drain current location and voltage width of the bench depends on the percentage of the nonuniformity and difference of the interface channel doping. The theoretical model has a bench similar to the actual power HEXFET in Figure 9.

A subthreshold bench can also occur in a discrete MOSFET, if one thinks of a single MOSFET as many MOSFETS in parallel. If an edge has a different subthreshold curve than the rest of the device, it could cause a bench in the subthreshold. Any nonuniform doping defect, which forms a continuous connection between the source

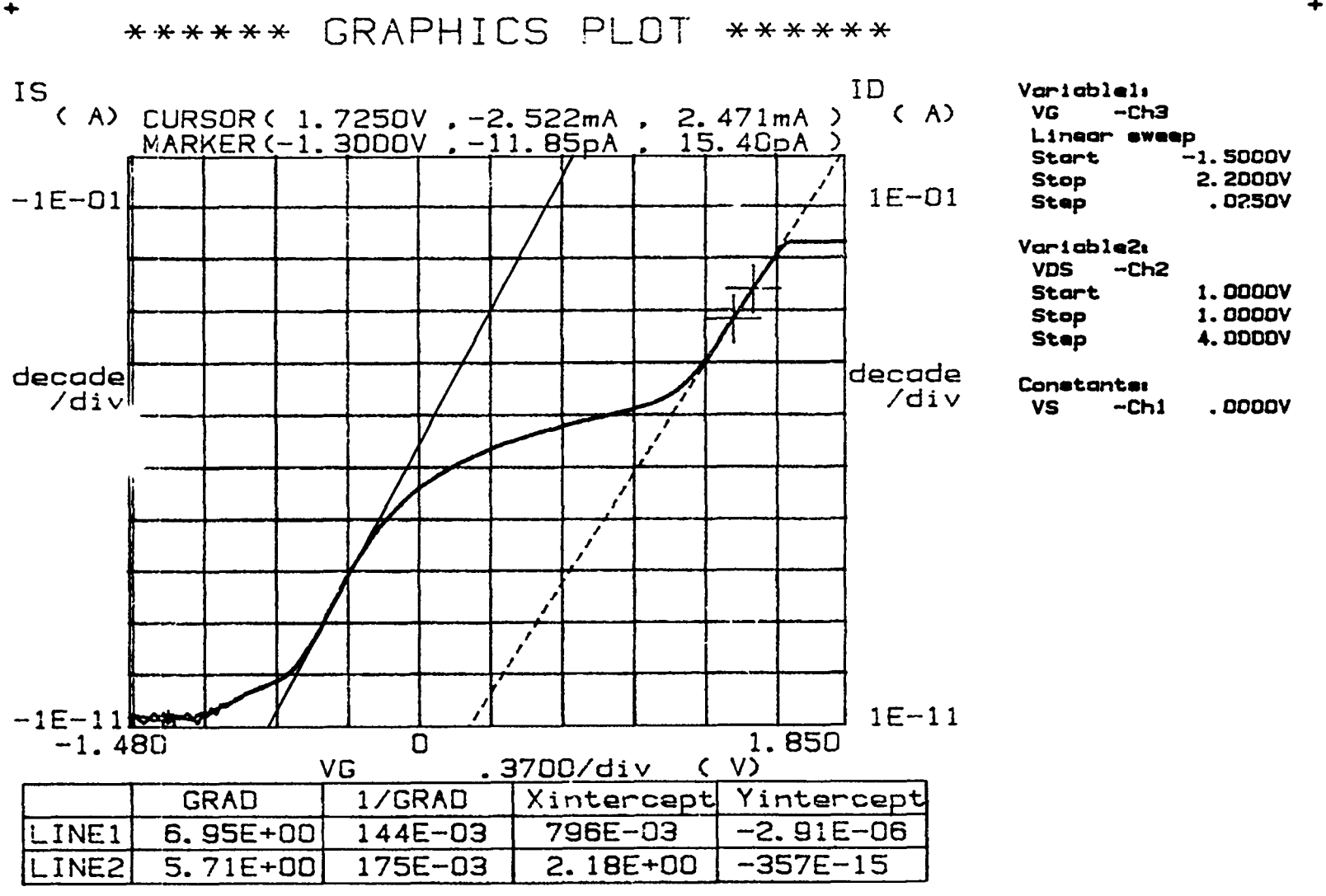

	GRAD	1/GRAD	Xintercept	Yintercept
LINE1	6.95E+00	144E-03	796E-03	-2.91E-06
LINE2	5.71E+00	175E-03	2.18E+00	-357E-15

Figure 9. Power HEXFET pre-irradiation subthreshold curve.

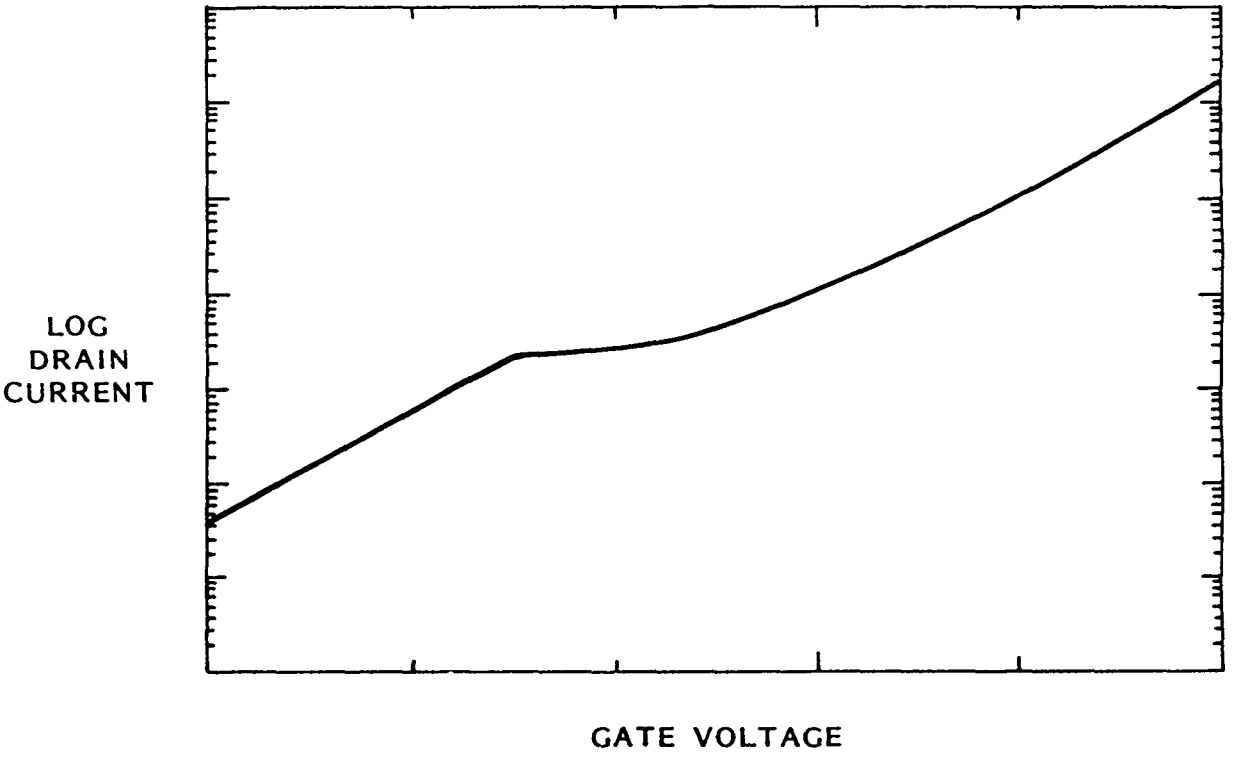

Figure 10. **Theoretical subthreshold curve for 10,000 transistors with 1.0 percent at 1.0×10^{14} cm^{-3} channel doping and the rest at 1.0×10^{16} cm^{-3}.**

and the drain, could also cause a bench. As was shown for the power HEXFET, these device parasitics can affect the subthreshold curve, even if they represent only 1.0 percent of the device width.

3.5.3 Subthreshold Effects in Insulated Substrate MOS Transistors.

The subthreshold characteristics of MOS transistors fabricated on insulating substrates (i.e., silicon-on-sapphire (SOS) and silicon-on- insulator (SOI)) are affected in three ways. These include: (1) backside leakage, (2) sidewall leakage, and (3) floating body effects. Backside leakage arises from a parasitic, a conducting path located at the interface between the epitaxial silicon and the insulator. This interface may be affected by charge trapped in the insulator or interface states existing at the boundary between the two materials. If the source/drain regions extend all the way to the silicon-insulator boundary, the pre-irradiation junction leakage is increased by the recombination/generation current at the interface. Post-irradiation leakage in an n-channel transistor is significantly increased because charge trapped in the insulator tends to invert the silicon near the boundary and creates a backside channel between the drain and source. The result is that the lower limit of subthreshold leakage current per unit width is initially higher in insulated substrate devices. In post-irradiation n-channel devices, the drain-to-source leakage can increase to the point that it obscures a significant portion of the top-side transistor subthreshold characteristic. In SOI technologies, the backside leakage path can be turned off by applying a negative potential to the silicon substrate.

Sidewall leakage arises from the parasitic MOS transistor formed at the ends of the intentional MOSFET. In mesa technologies, the gate extends over the edge of the silicon island and forms the parasitic transistor on a different silicon plane. The parasitic device may have a lower threshold voltage and be more susceptible to degradation because of a poorer quality gate oxide. A similar effect is found in technologies employing a trench for lateral device isolation. A parasitic transistor is formed where the source and drain abut the trench sidewall. The trench oxide is subject to fringing fields from the drain-to-source and may trap charge during

irradiation. The subthreshold characteristic of both mesa and trenched devices show changes in the subthreshold slope as a function of gate voltage. The turn-on of the parasitic transistor may entirely obscure the subthreshold characteristic of the top-side transistor. The sidewall transistor is eliminated in a closed geometry transistor in which the drain completely surrounds the gate and source so that the body never encounters the sidewall.

Floating body effects arise from the tendency of the body of the transistor to develop a forward bias with respect to the source. Leakage or avalanche currents from the drain to the body give rise to a body voltage which is clamped to one diode drop above the source voltage by the source-to-body diode. The result is to move the threshold voltage toward depletion through the body effect term which is a function of the square root of the body voltage. The strong inversion I/V characteristics exhibit a "kink" effect in the drain current versus drain voltage curves. The subthreshold characteristics are influenced by the shift of the strong inversion threshold voltage toward depletion. The net effect is to produce an effective change in slope in the portion of the curve near high injection as a function of drain voltage. In addition, subthreshold curves at different drain voltages tend to be offset toward depletion as the magnitude of the drain voltage increases. The floating body effect can be mitigated by providing source-to-body ties as part of the process.

3.6 CONCLUSIONS.

The overall result of the study of many the variables which affect the subthreshold curve is that the susceptibility of the subthreshold curve to these variables increases as the current decreases (excluding the kink effect). From this conclusion, extrapolation of nonideal characteristics (subthreshcld characteristics which are not described by equation (1)), which occur at small currents (roughly below 100 pA), is suspect. The nonideal variation may represent the action of some parasitic or defect in the device, which is only a small fraction of the total device. If this is true and the nonideal variation is extrapolated, the subthreshold charge separation technique would give results which are not representative of the bulk of the device. The midgap

voltage determined from this extrapolation would be the midgap voltage in the vicinity of the defect. The analysis would also be misleading in judging the radiation hardness of the gate oxide. From an engineering view, the extrapolation of this nonideal variation still would not be justified. Nonlinear subthreshold currents at or below 100 pA would not usually contribute to the failure of a circuit function.

To minimize the effects from variables which cause nonideal subthreshold curves at low currents, the upper part of the subthreshold should be extrapolated.

SECTION 4

APPLICATION

In order to apply the subthreshold charge separation technique, the following data set and parameters must be known:

1. The drain and/or source current (which best represents the channel current) versus gate voltage for gate voltages corresponding to below midgap through strong inversion. This data set may be taken either in the linear or saturated region provided $V_D \gg kT/q$.
2. Measurement of mobility.
3. Gate oxide thickness.
4. Interface channel region doping density.

4.1 MEASUREMENT OF $I_D(I_o)$ versus V_G.

For a perfect MOSFET, the drain current will be composed almost entirely of the channel current under the gate. In this case, the drain current will follow an exponential dependence on gate voltage in the subthreshold with a single valued slope and will yield ideal MOSFET subthreshold characteristics. In real MOSFETs, there are several other components of drain current that will result in a departure from the ideal subthreshold curve. These components include drain to substrate leakage, gate leakage, edge or sidewall leakage and back channel leakage. The edge or sidewall leakage can occur under a field oxide or an extension of the gate oxide. Both sidewall and back channel leakage may be present in CMOS/SOS or CMOS/SOI technologies. A technique for reducing the interference from leakage sources is to measure the source current, I_S, rather than the drain current, I_D. This will eliminate the drain to substrate leakage current, since source and substrate are usually common, and it

may reduce other leakage components as well. Before a decision is made whether to monitor I_D versus V_G, or I_S versus V_G, the currents in all available leads of the MOSFET should be monitored as a function of V_G on the unirradiated samples.

The test configuration for the measurement of channel current versus gate voltage is shown in Figure 11 for an n-channel MOSFET. The test transistor should have all four regions with separate contacts if possible. For many technologies, this may not be possible. For example, in power MOSFETs the source and substrate are usually shorted with metallization on the chip. In CMOS/SOS and CMOS/SOI, the substrate is often floating. In these cases only three terminals will be available. If measurements are being performed on, a) test transistors located on process control or radiation effects test chips, or b) test transistors located on actual microcircuit die, the test transistors should be designed for access to all four regions.

4.1.1 Preliminary Device Characterization.

In order to determine whether the drain or source subthreshold characteristics best represent the channel current, a preliminary test should be conducted on several unirradiated samples to determine the magnitude of the leakage components and the shape of the subthreshold curve. If all four regions are bonded out separately, then the drain current, I_D, the source current, I_S, the gate current, I_G, and the substrate current, I_B, should be measured as a function of the gate voltage from below midgap to strong inversion. An example of such a data set is shown in Figure 12 for a silicon gate n-channel MOSFET representative of a 3 μm bulk CMOS process. In this figure, plotted directly from the graphic output of the HP4145, all four terminal currents are shown for both linear ($V_D = 0.1$ V) and saturated ($V_D = 10$ V) operation. The top trace in the inversion region is I_D at $V_D = 10$ V. Going down the graph, the second curve is I_S at $V_D = 10$ V, followed by I_B at $V_D = 10$ V. The fourth curve down is both I_D and I_S at $V_D = 0.1$ V, and the bottom trace is composed of three curves, I_B at $V_D = 0.1$ V and I_G at both $V_D = 10$ V and 0.1 V. Because of the large value of I_B at $V_D = 10$ V, the source current is a much better representation of the channel current than the drain current, which is the sum of channel and bulk current. Although this

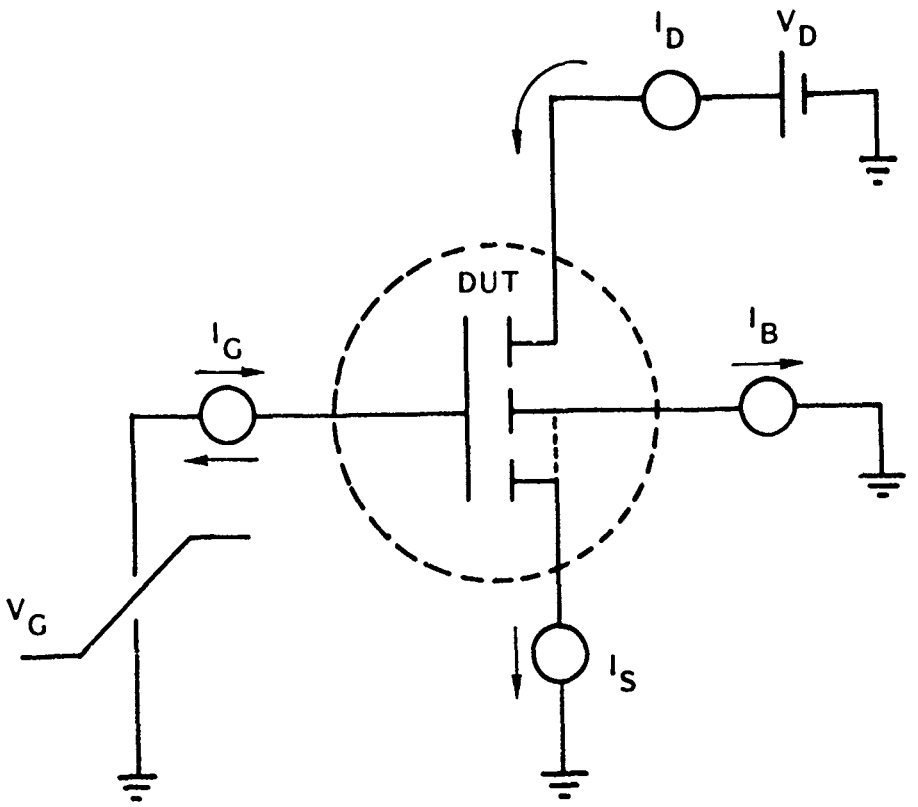

Figure 11. Test configuration for measurement of $I_D(I_S)$ versus V_G.

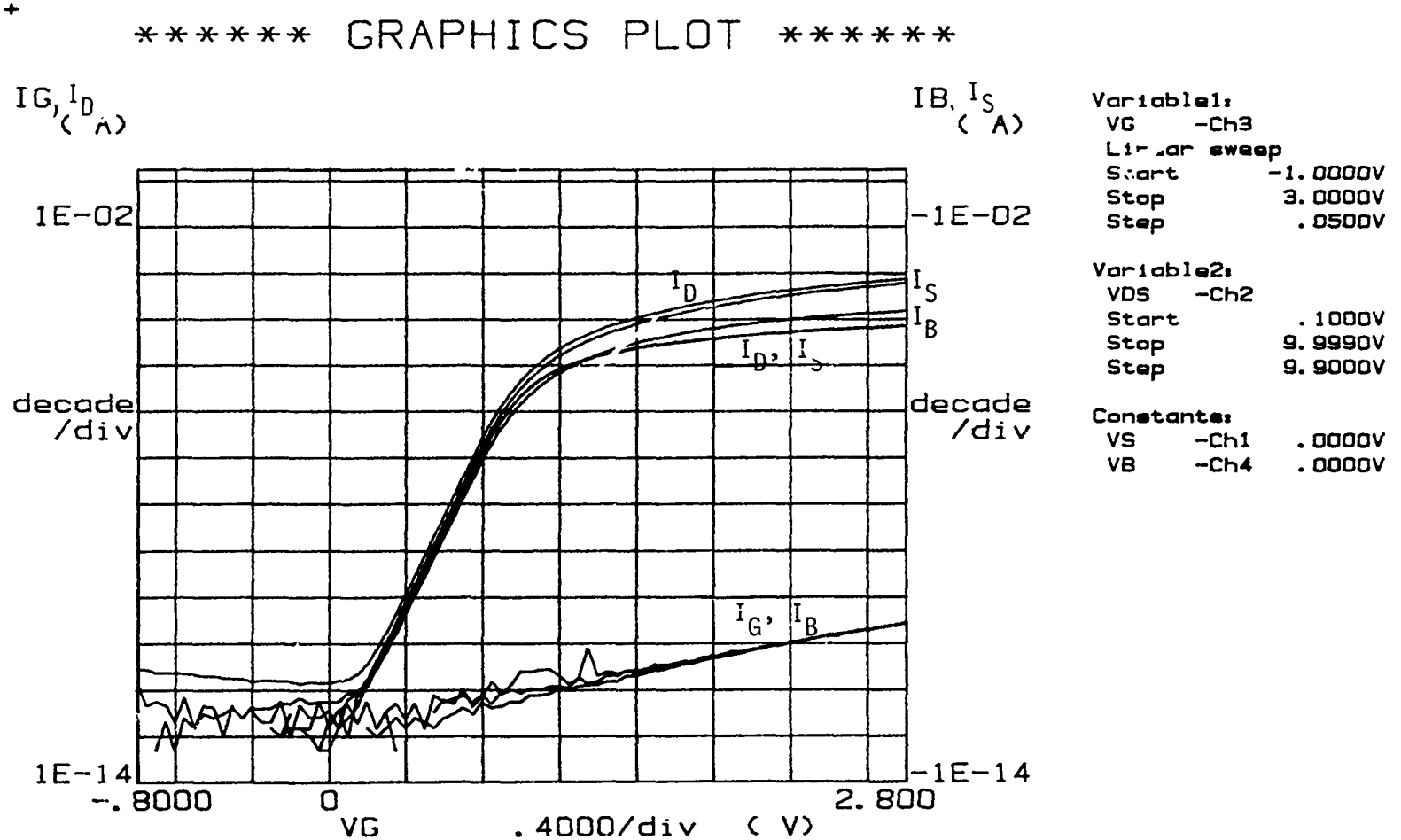

Figure 12. Plot of all four terminal currents for linear and saturated operation.

difference can be observed in pre-irradiation curves taken in saturation, it is much more pronounced in post-irradiation curves where the drain to substrate leakage has increased due to the surface effects around the periphery of the drain. If bulk or substrate leakage currents are appreciable, the source current is a better measure of the channel current. However, if there is any appreciable gate leakage, the gate may leak to the source causing a distortion of the source curve. This is illustrated in Figure 13, which shows all four terminal currents at $V_D = 0.1$ V and 5 V for a p-channel device. The source current follows the gate leakage current in subthreshold, whereas the drain current is a good measure of the channel current. For $V_G = 0$ V to ~0.8 V, the gate current and bulk current are equal in magnitude, implying that in this range of operation, the gate leaks to the bulk. In Figure 14, the four terminal currents of an n-channel device are shown illustrating a large gate leakage current. In this case, the gate leaks to the substrate and the source and drain current are unaffected. Thus, if all four terminals are available, I_S and I_D are near ideal, and the charge separation technique would apply. However, if this were a three terminal device with the source and substrate tied together internally, I_S and I_D would no longer be equal. This is illustrated in Figure 15, which is the same device with the source and substrate shorted together at the device pins. In this case, the source current follows the gate leakage current until the channel current becomes large compared to the gate leakage. For a three terminal version of this device, the drain current should be used to represent the channel current.

The above examples illustrate how the gate and substrate leakage currents can affect the source and drain currents in subthreshold. Therefore, it is necessary to fully characterize the currents in all available device leads before deciding whether to perform data analysis on the source current or drain current.

4.1.2 Pre- and Post-Irradiation Measurement of Channel Current Versus Gate Voltage.

Once the preliminary characterization has been performed to determine whether the source or drain current is more representative of channel current, a pre-

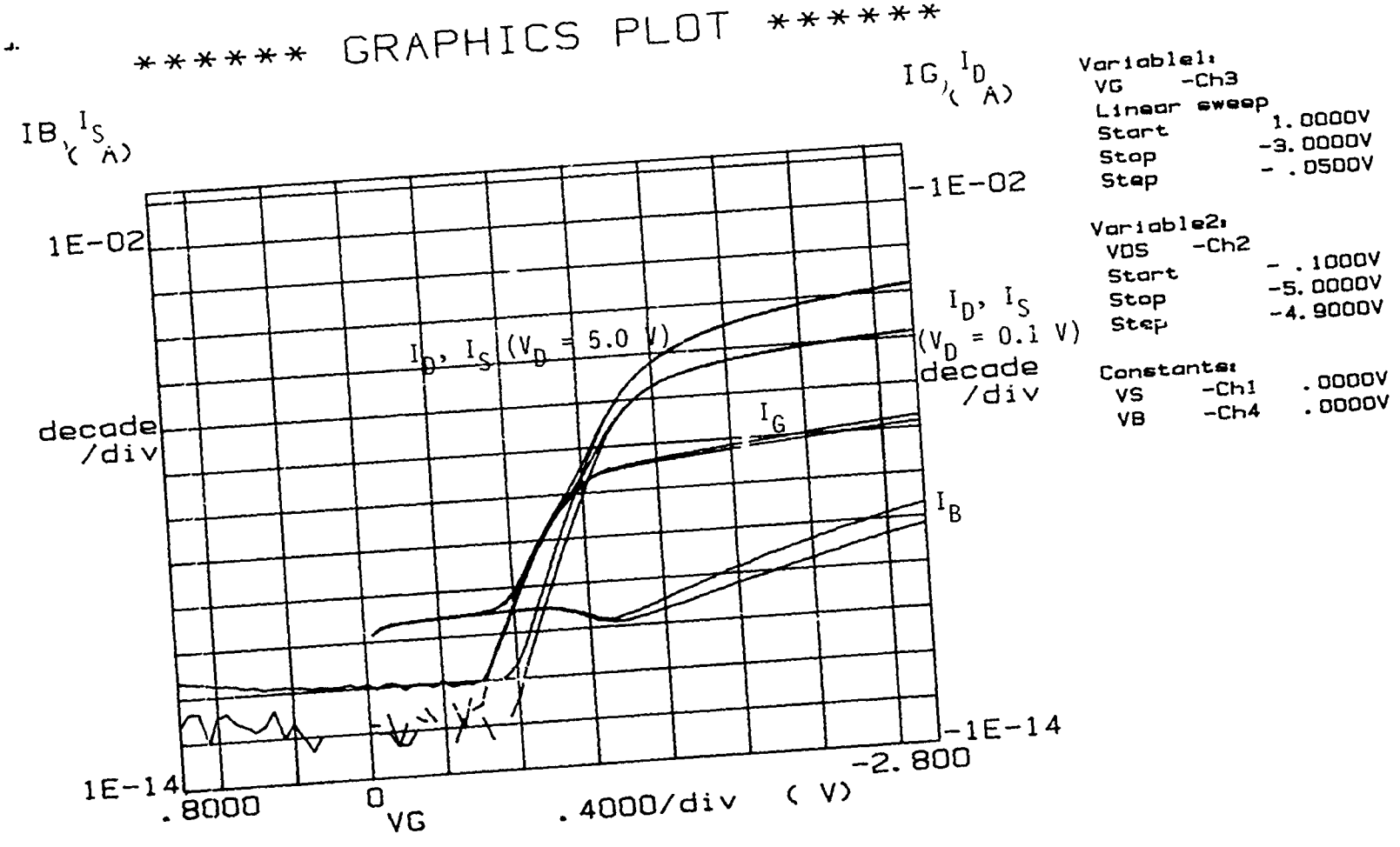

Figure 13. **Terminal currents for a p-channel device showing gate leakage to the source.**

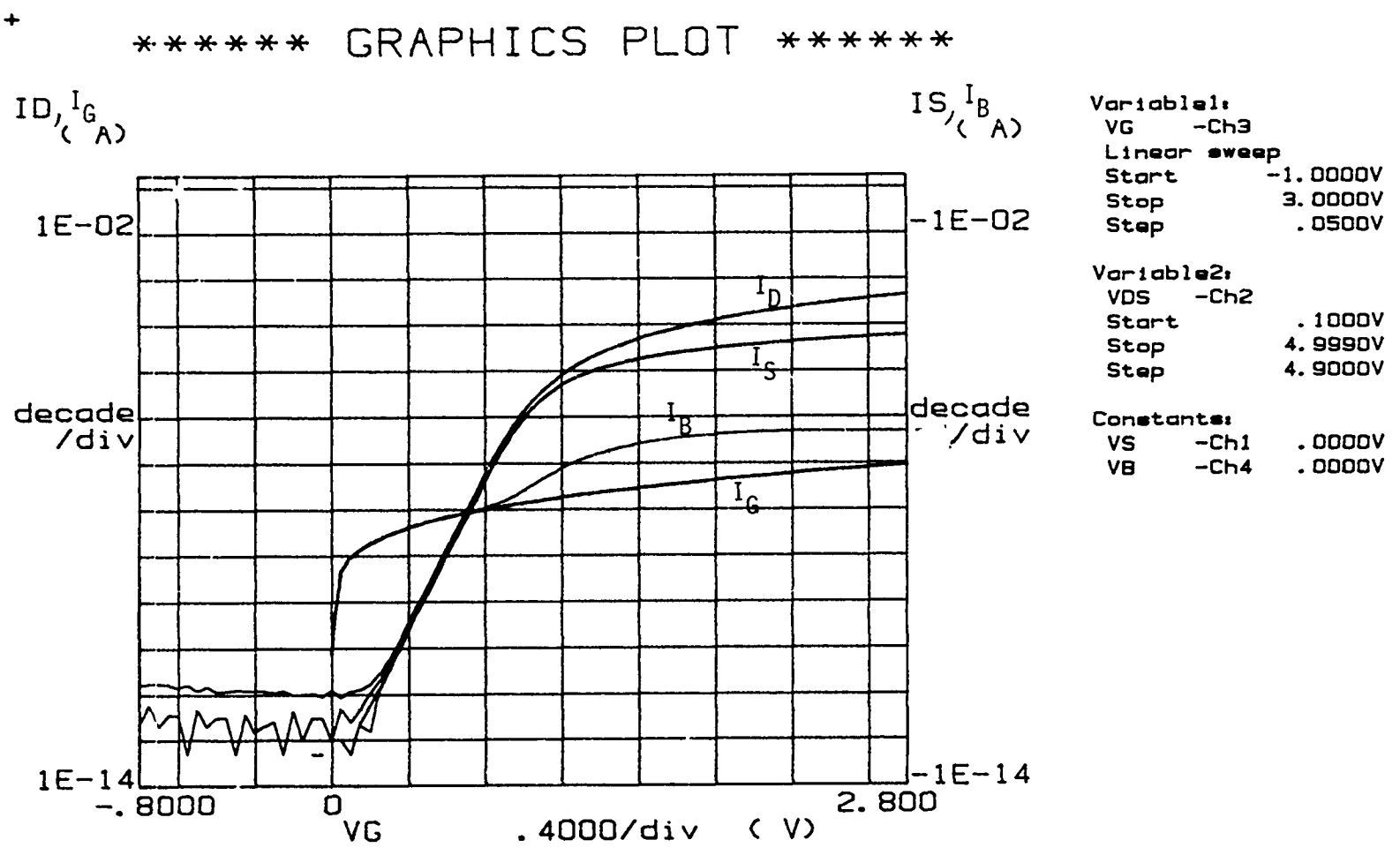

Figure 14. Terminal currents of an n-channel MOSFET showing gate leakage to substrate.

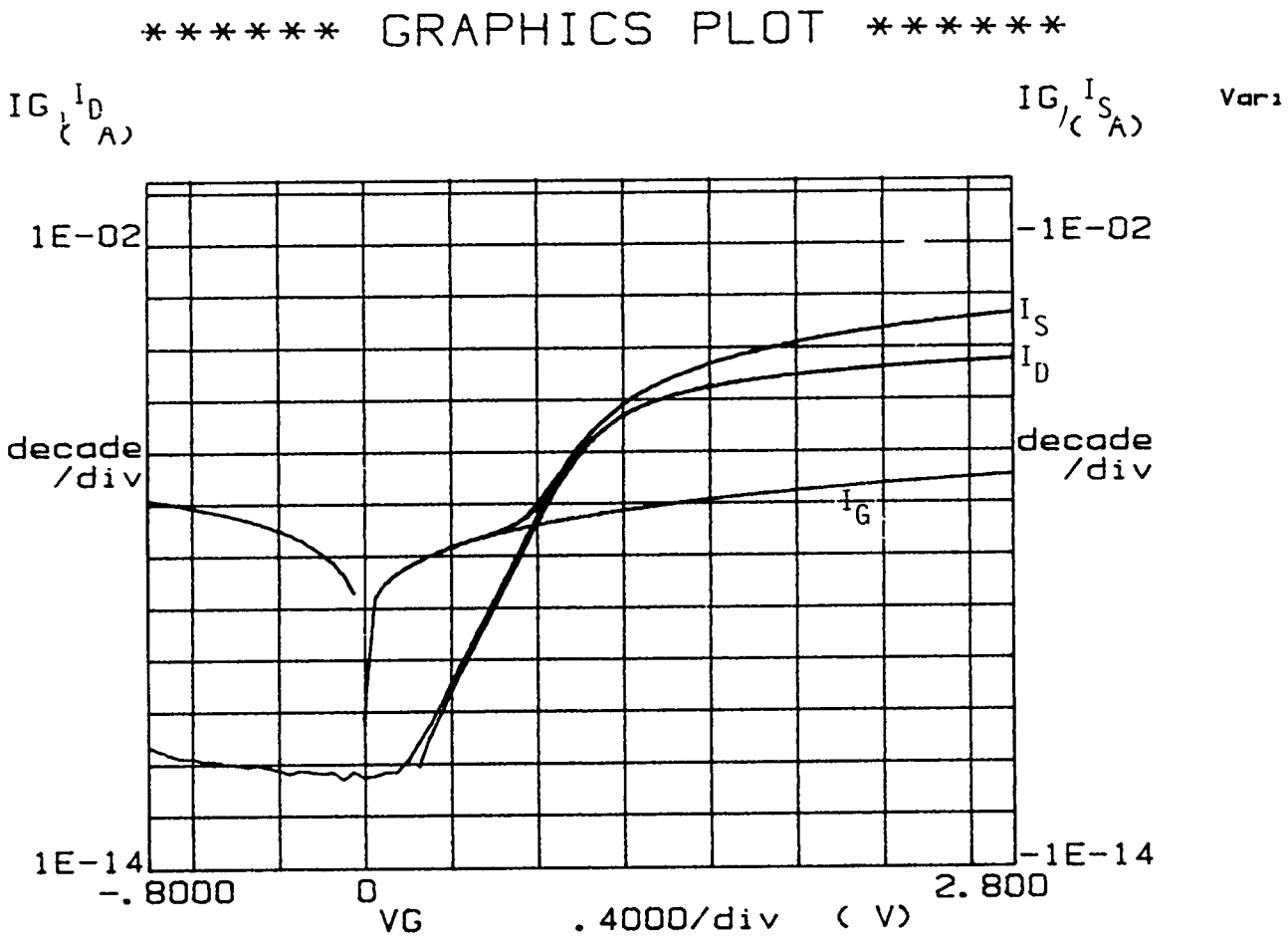

Figure 15. **Same plot as previous figure with substrate and source shorted at device pins.**

irradiation characteristic is measured. The measurement of $I_D(I_S)$ versus gate voltage should be taken from below midgap to strong inversion. The drain voltage can be set for either linear or saturated operation in inversion. If drain voltage is set for linear operation, the condition $V_D \gg kT/q$ must be satisfied. At room temperature, V_D should be at least 100-150 mV. For saturated operation, V_D can be set at the maximum operating voltage.

There are several precautions that should be considered for saturated operation:

1. Short channel effects are maximized for large drain voltage;
2. Hot electron effects may occur for large drain voltage;
3. Drain to substrate currents may be significant for large drain voltage. This effect is illustrated in Figures 13 and 15;
4. In floating substrate technologies such as CMOS/SOS and CMOS/SOI the kink effect may occur for large drain voltage;
5. In devices with $V_{T_L} > V_D(MAX)$ saturated operation is not possible. An example is a field oxide MOSFET with relatively high interface doping density; and
6. Measurement of mobility.

Because of the above limitations, it is recommended that the subthreshold characteristic be measured in the linear region with 100 mV$< V_D <$500 mV.

4.2 MEASUREMENT OF MOBILITY.

To apply the subthreshold charge separation technique, a value for the channel mobility is required and, therefore, a measurement of the transconductance of the device is needed. The transconductance of a MOSFET theoretically depends on

whether the device is in the linear or saturation region. In the linear region, the transconductance, G_M, is given by

$$G_M = \frac{Z}{L}\mu C_{oz} V_D, \tag{31}$$

and in the saturation region,

$$G_M = \frac{2mZ}{L}\mu C_{oz}\left(V_G - V_{TH}\left(V_{INV}\right)\right), \tag{32}$$

where m is a function of doping concentration and approaches 0.5 at low doping. Both equations (31) and (32) could be used to determine coefficients for the drain current of equation (1). From the transconductance, the value of the term, K, needed for equation (1) is

$$K = \frac{G_M}{V_D} = \frac{Z}{L}\mu C_{oz} \quad \text{for the linear region,}$$

or

$$K = \frac{G_M}{2m\left(V_G - V_{TH}\left(V_{INV}\right)\right)} = \frac{Z}{L}\mu C_{oz} \quad \text{for the saturation region.} \tag{33}$$

For the linear region, one just divides the transconductance by the applied drain voltage that was used to make the measurement.

Transconductance is a function of the drain and gate voltages applied. The drain voltage has a direct effect, but also has an indirect effect in the channel length. The mobility is a strong function of the gate voltage due to the vertical electric field, as was discussed previously. In the subthreshold charge separation technique, a mobility is needed which represents the weak inversion value. Since, for a MOSFET, the mobility increases as the surface potential is lowered, the maximum strong inversion value should be used. In strong inversion, Figure 16 shows the mobility decreasing as gate voltage is increased for a 3 μm bulk CMOS technology n-channel. This is an important consideration in making linear region transconductance measurements. Figure 17 shows the value, K, for drain voltages of 0.1 and 5.0 volts. When the drain is at 5.0 volts, the value of K is decreased by almost a factor of 3 which is caused by the decrease in mobility. In this device, the effect of a decreased channel length is

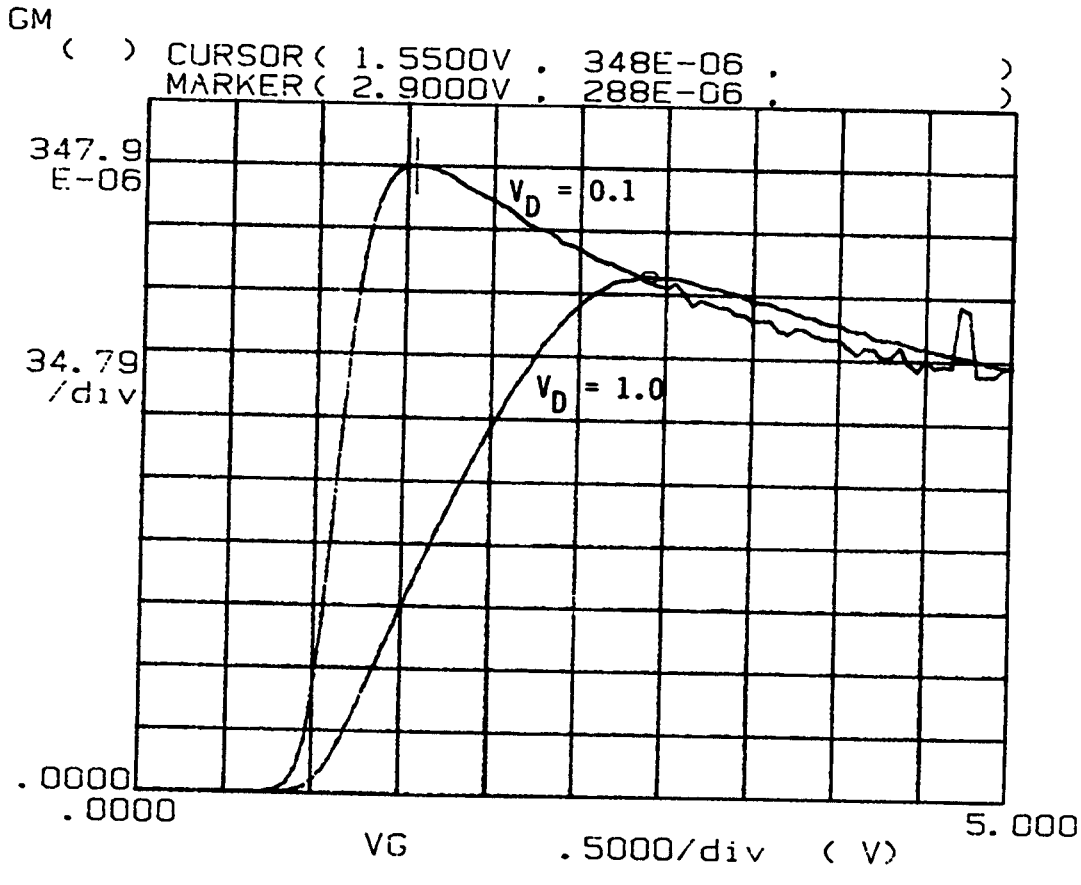

Figure 16. Plot of K versus gate voltage in the linear region for drain voltages of 0.1 and 1.0 volt.

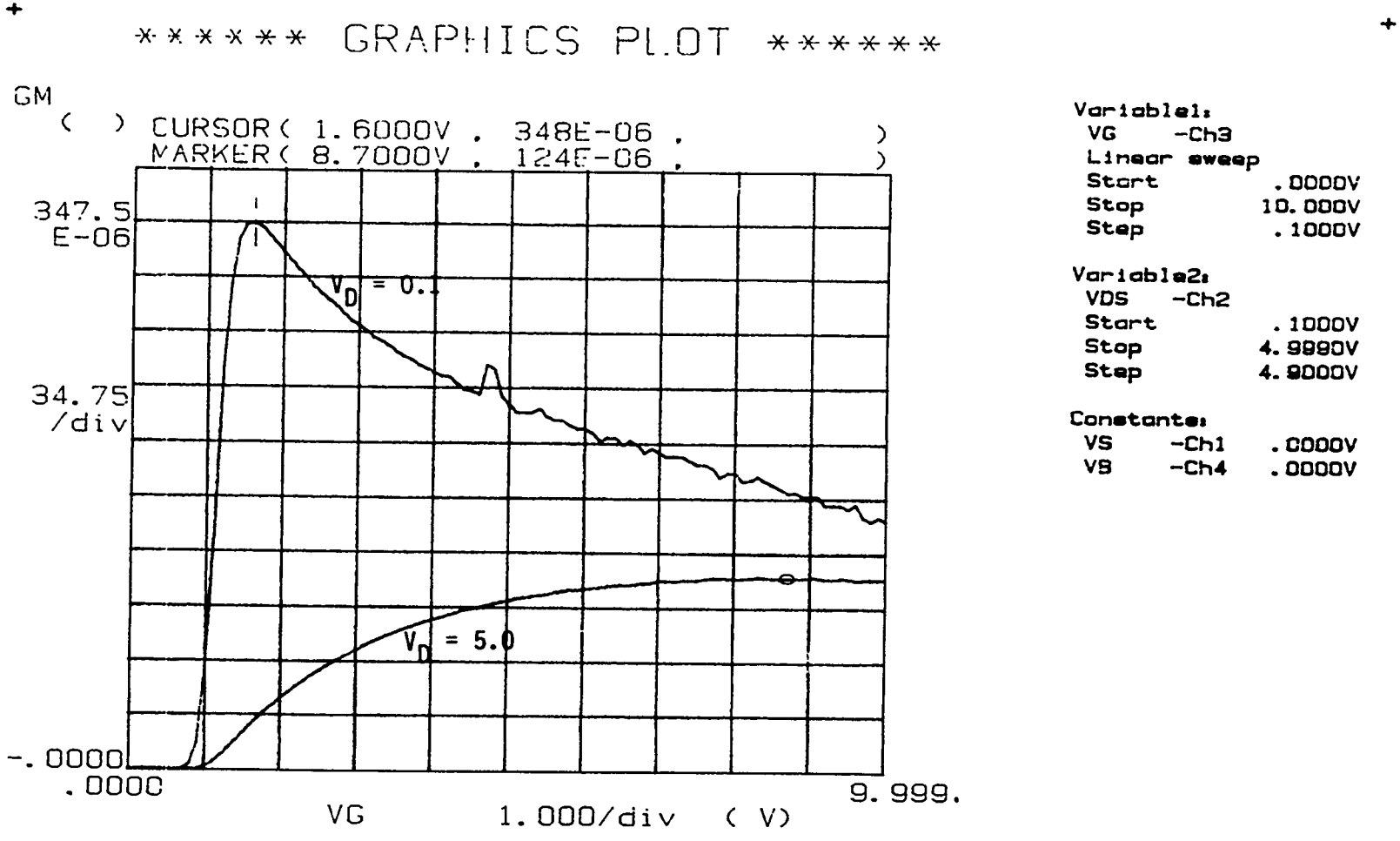

Figure 17. Plot of K versus gate voltage in the linear region for drain voltages of 0.1 and 5.0 volts.

dominated by the decrease in mobility. This implies that the mobility in the linear region at a drain voltage of 5 volts has already substantially been degraded by the gate voltage. Comparing 0.1 to 1.0 volt in Figure 16, the decrease in mobility is only about 15 percent. For this process, linear region mobility degradation due to the gate electric field does not sharply increase until the drain voltage is larger than 1.0 volt.

Saturation transconductance, equation (32), can also be used to evaluate the coefficient for the drain current. This technique does not seem to yield the maximum values that are obtained in the linear region. Figure 18 shows the use of equation (32) for the same device used to generate Figures 16 and 17. The mobility term is 30 percent lower when determined using the saturation region.

Mobility is needed to calculate the midgap and inversion currents. Since interface states degrade the mobility, it is expected that post-irradiation mobility will be less than the pre-irradiation value. The subthreshold charge separation technique has been done using the pre-irradiation mobility to analyze the post-irradiation data, and recalculating the mobility for each post-irradiation data set. If the pre-irradiation value is used, one assumes that: 1) the weak inversion mobility changes little with irradiation, or 2) the mobility calculated from the post-irradiation curves are a worse estimate of the post-irradiation weak inversion mobility than the pre-irradiation calculated mobility.

Using the interface state neutrality assumption, the mobility at midgap is better approximated by the pre-irradiation value. At midgap, all interface states located above midgap have neutral charge, and it is assumed that there are not many trapped holes near the interface to affect the mobility.

Thus, for the calculation of the midgap current, the nondegraded pre-irradiation value should be used. For post-irradiation, the mobility is assumed to be degraded by interface states, and at the inversion voltage, it is also assumed that all interface states are charged. Thus, the value of mobility at the post-irradiation inversion voltage may be better represented by the mobility calculated from that data set. If a measured threshold voltage is used, only the pre-irradiation transconductance needs to be

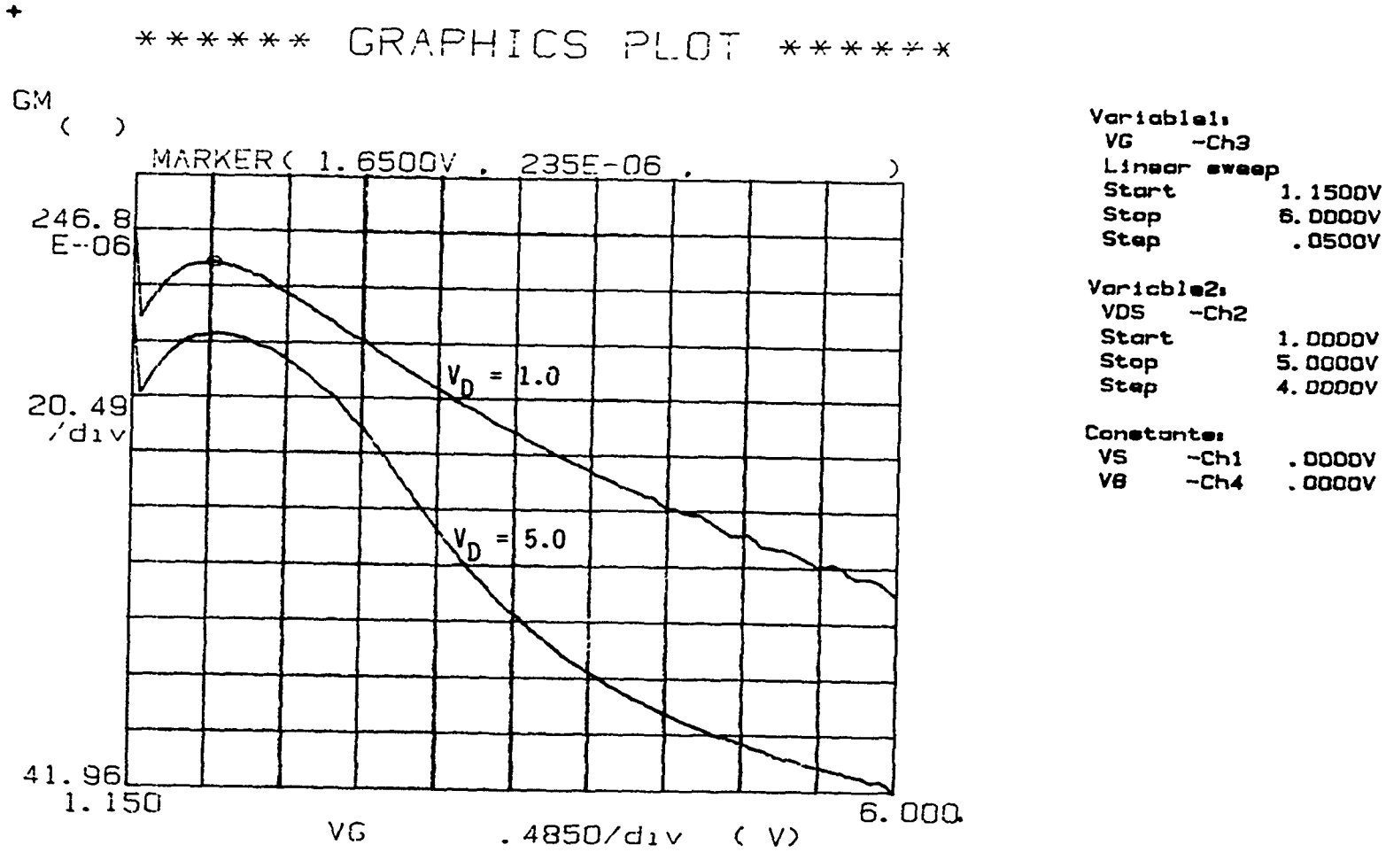

Figure 18. Plot of K versus gate voltage in the saturation region for drain voltages of 1.0 and 5.0 volts.

measured. If the inversion current is calculated, then both pre- and post-irradiation mobilities could be measured and used in the data analysis.

To achieve the best estimates for the mobilities at midgap and post-irradiation inversion, the smallest possible drain voltage should be used. This enables the mobility to be measured at small gate voltages and, thereby, minimizes the surface roughness and electric field effect. Also, the mobility would be measured at a gate voltage close to inversion providing a better estimate of the actual weak inversion mobility. For pre-irradiation data where interface state concentration is small, the mobility should be degraded very little at small gate voltage. If this degradation is small, the measured mobility should be close to the actual mobility at midgap.

4.3 DATA ANALYSIS.

As stated earlier, the subthreshold charge separation technique can be used either as an engineering tool to compare the threshold voltage shift contributions from trapped holes, ΔV_{OT}, and interface states, ΔV_{IT}, or it can be used as a research tool to determine the energy density of the interface states, D_{IT}. For use as an engineering tool to either characterize technologies, investigate process hardening techniques or perform hardness assurance, the data analysis is quite straightforward. However, if the technique is to be used as a research tool to explore the spatial dependence of trapped holes or the energy dependence of the interface states, the data requirements are more severe and the analysis more complicated.

4.3.1 Separation of ΔV_{TH} into ΔV_{OT} and ΔV_{IT}.

The data analysis procedure for the separation of ΔV_{TH} into the components ΔV_{OT} and ΔV_{IT}, is based on the following equations as discussed in Section 2,

$$\Delta V_{OT} = \Delta V_{MG},$$

and

$$\Delta V_{IT} = \Delta V_{TH} - \Delta V_{OT},$$

or

$$\Delta V_{IT} = \left(\frac{q\phi_B}{kT\ell n10}\right)\Delta S,$$

and

$$\Delta V_{OT} = \Delta V_{TH} - \Delta V_{IT}.$$

Using the midgap method, the midgap voltage shift, ΔV_{MG}, is calculated from the pre- and post-irradiation subthreshold log I_D versus V_G characteristics using the following procedure:

1. 1) Determine the value of $\frac{Z}{L}\mu C_{oz} = \frac{G_M}{V_D}$ from a calculation of peak transconductance, $\Delta I_D/\Delta V_G$ using the pre-irradiation I_D versus V_G data in strong inversion as shown previously in Figure 16.
2. Obtain values of the oxide thickness, t_{oz}, and the channel (substrate) doping, N_A or N_D.
3. Calculate the channel midgap current, I_{MG}, from equation (12) and (1) of Section 2.
4. Extrapolate the straight line pre-irradiation subthreshold log I_D versus V_G characteristic to a value I_{MG}. The gate voltage at I_{MG} is V_{MGI}.
5. Extrapolate the straight line post-irradiation subthreshold log I_D versus V_G characteristic to the same value I_{MG}. This gate voltage is $V_{MG\gamma}$.
6. $\Delta V_{MG} = V_{MG\gamma} - V_{MGI} = \Delta V_{OT}$.
7. Repeat 5) and 6) for each post-irradiation subthreshold characteristic.

Because the oxide trapped holes due to irradiation is positive, ΔV_{OT} will always be negative.

Using the subthreshold swing method, the voltage shift due to interface states, ΔV_{IT} is calculated from the pre- and post-irradiation log I_D versus V_G characteristics using the following procedure:

1. Obtain the value of channel (substrate) doping, N_A or N_D.
2. Calculate the straight line fit to the pre-irradiation log I_D versus V_G subthreshold characteristics.
3. Calculate straight line fit to the post-irradiation Log I_D versus V_G subthreshold characteristics.
4. $\Delta S = S_\gamma - S_I$.
5. $\Delta V_{IT} = (q\phi_B/kT\ell n10)\,\Delta S$
6. Repeat 3), 4), and 5) for each post-irradiation subthreshold characteristic.

In order to calculate the value of ΔV_{IT} using the midgap method, or ΔV_{OT} using the subthreshold swing method, the irradiation induced threshold voltage shift ΔV_{TH} or the inversion voltage shift, ΔV_{INV} must be determined. The value of ΔV_{TH} is simply

$$\Delta V_{TH} = V_{TH\gamma} - V_{THI},$$

where V_{THI} is the pre-irradiation value of V_{TH} and $V_{TH\gamma}$ is the post-irradiation value of V_{TH}. The threshold voltage is the extrapolated gate voltage for $I_D = 0$ using either a plot of $\sqrt{I_D}$ versus V_G for operation in saturation or a plot of I_D versus V_G for operation in the linear region. The calculation of V_{TH} is illustrated in Figures 19 and 20.

The value of ΔV_{INV} is calculated using equation (7) and the following procedure:

1. Determine the value of $\frac{Z}{L}\mu C_{oz} = \frac{G_M}{V_D}$ from a calculation of peak transconductance, $\Delta I_D/\Delta V_G$ using the pre-irradiation I_D versus V_G data in strong inversion as shown previously in Figure 16.

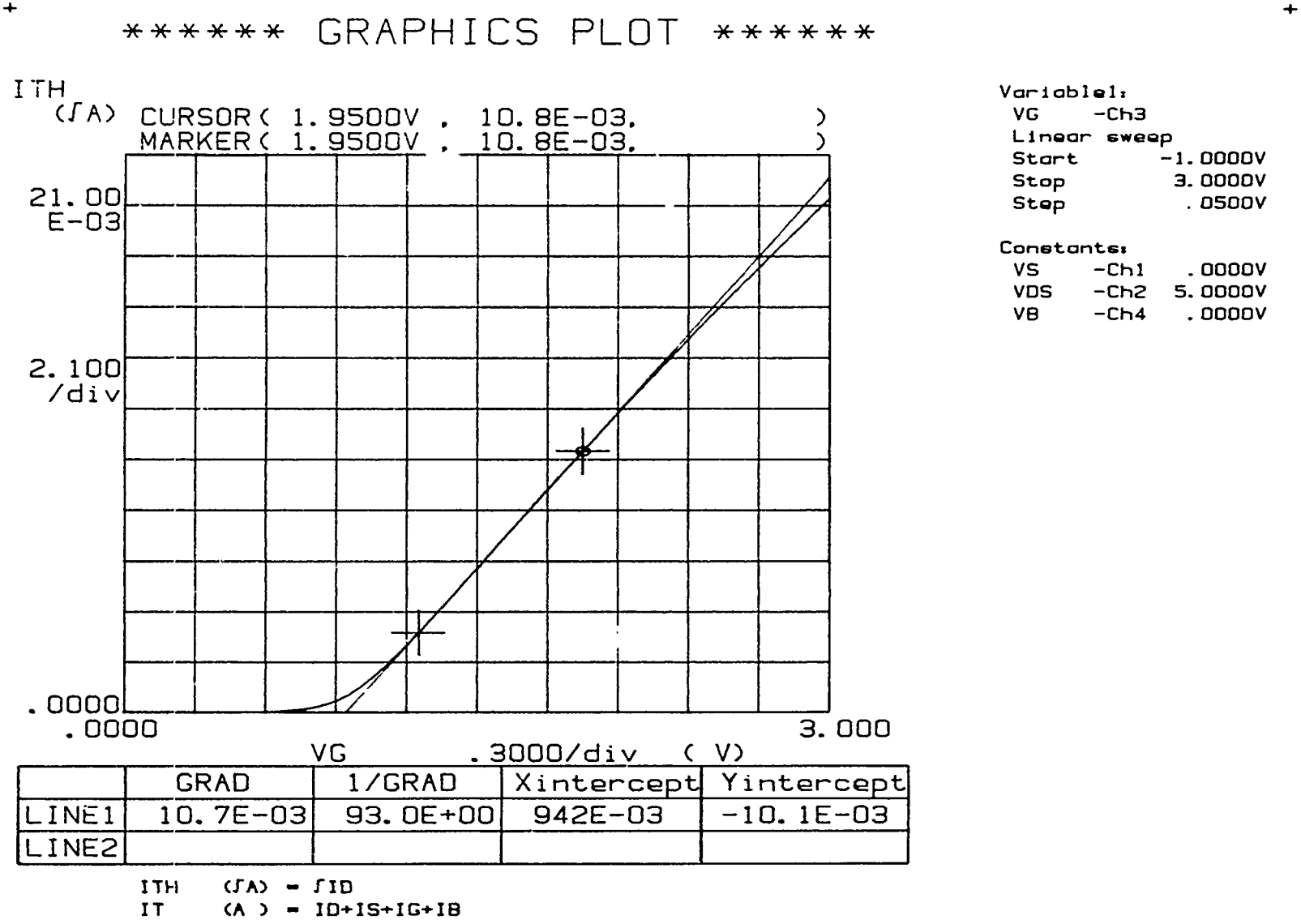

	GRAD	1/GRAD	Xintercept	Yintercept
LINE1	10.7E-03	93.0E+00	942E-03	-10.1E-03
LINE2				

Figure 19. Threshold voltage determination from plot of $\sqrt{I_D}$ versus V_G for saturated operation with $V_D = 5$ V.

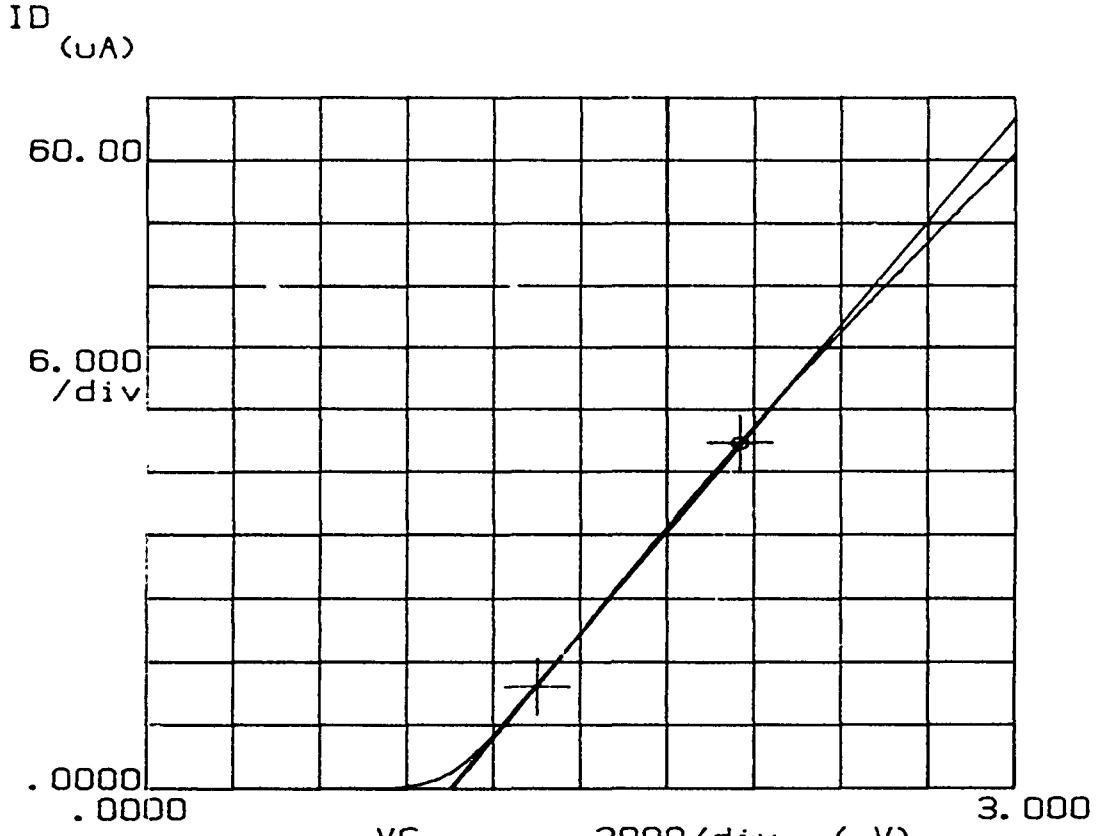

	GRAD	1/GRAD	Xintercept	Yintercept
LINE1	33.0E-06	30.3E+03	1.06E+00	-34.9E-06
LINE2				

ITH (A) = ∫ID
IT (A) = ID+IS+IG+IB

Figure 20. Threshold voltage extrapolation from plot of I_D versus V_G for linear operation with $V_D = 0.1$ V.

2. Obtain values of the oxide thickness, t_{ox}, and the channel (substrate) doping, N_A or N_D.

3. Calculate the channel inversion current, I_{INV}, from equation (7).

The value of ΔV_{INV} is

$$\Delta V_{INV} = V_{INV\gamma} - V_{INVI}.$$

where V_{INVI} is the pre-irradiation value of V_{INV} and $V_{INV\gamma}$ is the post-irradiation value.

In p-channel devices, ΔV_{TH} will always be negative since the net charge of the interface states is positive, causing ΔV_{IT} to be negative. In n-channel devices, where the net charge of the interface states is negative, ΔV_{IT} will be positive. Therefore, in n-channel devices, ΔV_{TH} may be positive or negative depending on whether $|\Delta V_{IT}|$ is larger or smaller than $|\Delta V_{OT}|$.

If the midgap method is used, ΔV_{IT} is calculated by

$$\Delta V_{IT} = \Delta V_{TH}(\Delta V_{INV}) - \Delta V_{OT}.$$

If the subthreshold swing method is used, ΔV_{OT} is calculated by

$$\Delta V_{OT} = \Delta V_{TH}(\Delta V_{INV}) - \Delta V_{IT}.$$

Figure 21 is an illustration of a typical pre- and post-irradiation plot of log I_D versus V_G for an n-channel MOSFET showing the separation of ΔV_{TH} into ΔV_{OT} and ΔV_{IT}. In Figure 22, a p-channel pre- and post-irradiation subthreshold characteristic are shown.

Although the midgap method of the subthreshold voltage separation technique can be applied graphically as shown in the examples, for large data sets, a computer program should be written to perform the necessary calculations. The only input data required for such a program are the (I_D, V_G) point pairs, the drain voltage, V_D, and the parameters t_{ox} and N_A or N_D for the calculation of midgap and inversion voltages.

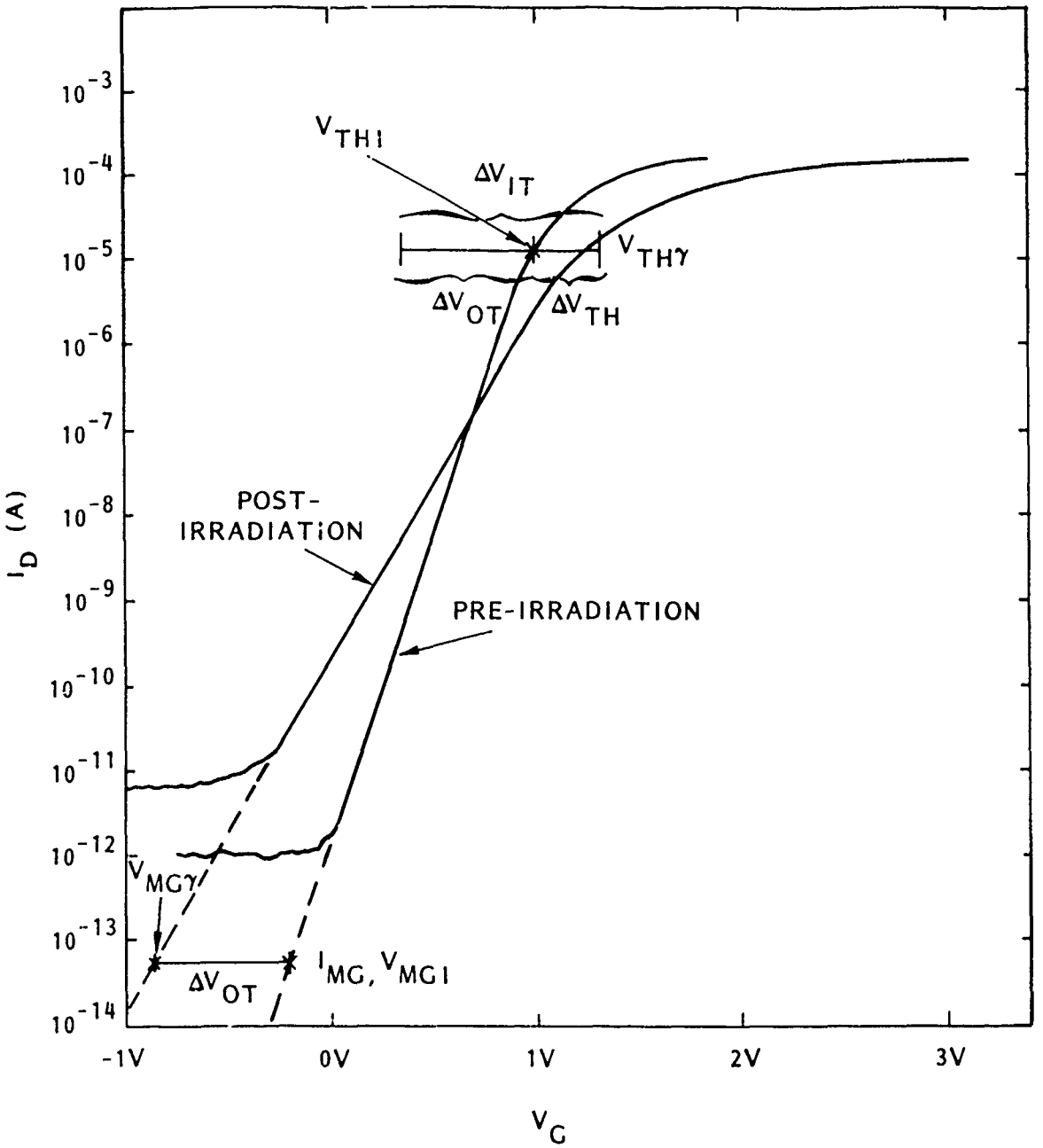

Figure 21. Typical voltage shift separation for n-channel device.

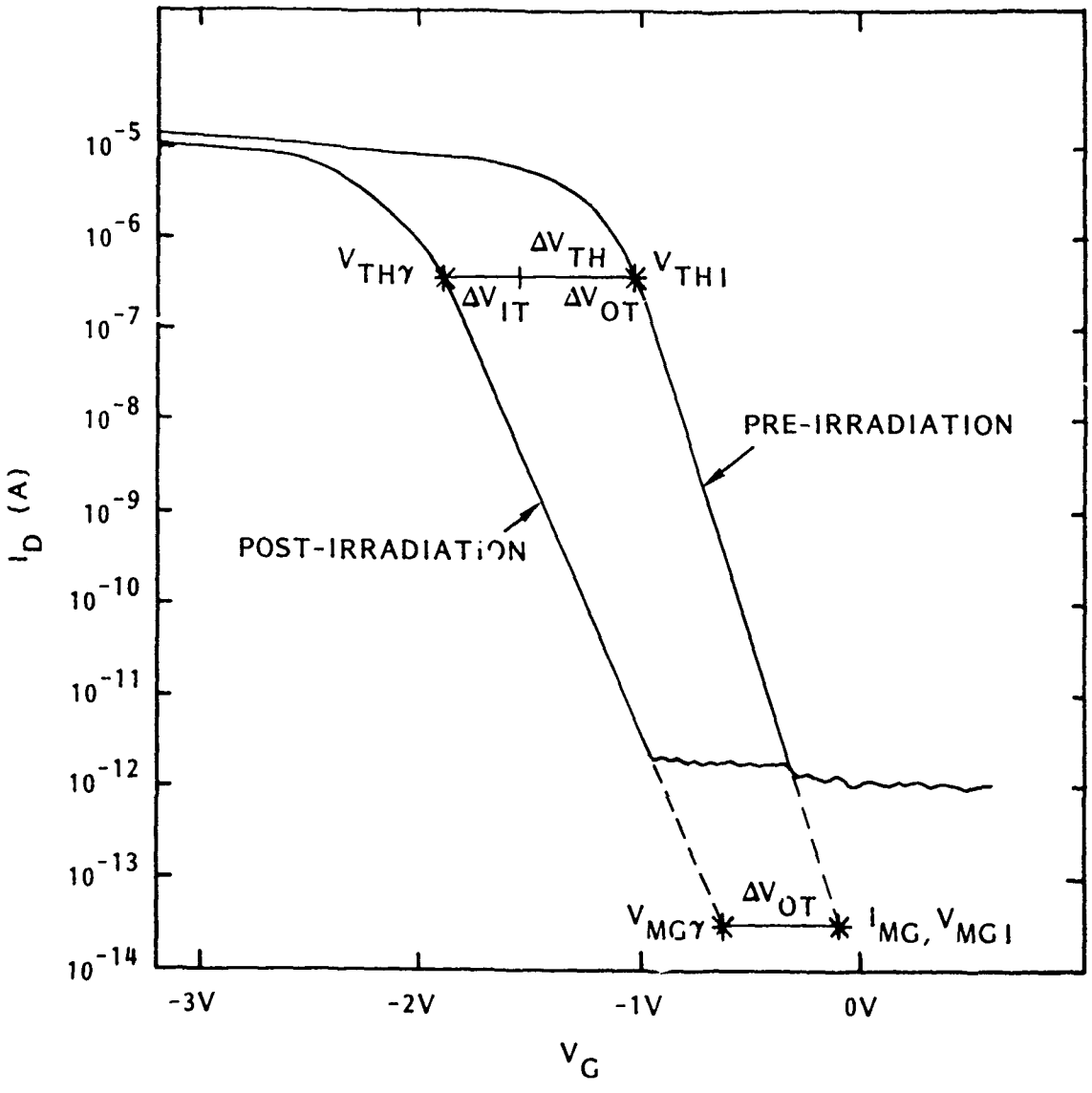

Figure 22. Typical voltage shift separation for p-channel device.

4.3.2 Use of Subthreshold Data for Determination of ΔN_{OT} and ΔN_{IT}.

The subthreshold technique can also be used for the investigation of irradiation induced oxide trapped charge, ΔN_{OT}, and the energy density of the interface states, D_{IT}, or its integrated value from midgap to inversion, ΔN_{IT}. The value of ΔN_{OT} can be obtained from ΔV_{MG} provided certain assumptions can be made about the spatial distribution of the trapped holes. A value of D_{IT} versus gate voltage (surface potential) can be calculated provided certain assumptions are made concerning the subthreshold mobility.

If the net charge of the interface states at midgap is zero,[4] the voltage shift, ΔV_{MG}, is due entirely to the irradiation induced trapped hole density in the gate oxide. Therefore,

$$\Delta V_{MG} = \frac{-1}{\epsilon_{ox}} \int_o^{t_{ox}} \Delta\rho_{ox}(x) x dx \tag{34}$$

where $\Delta\rho_{ox}(x)$ is the spatial positive charge density in the oxide, t_{ox} the oxide thickness and x is measured from the silicon/silicon dioxide interface to the gate. If $\Delta\rho_{ox}$ is a sheet charge next to the silicon containing $q\Delta N_{OT}$ charges, $\Delta V_{MG} = q\Delta N_{OT}/C_{ox}$; and if $\Delta\rho_{ox}$ is a constant equal to $q\Delta N_{OT}$, $\Delta V_{MG} = q\Delta N_{OT}/2C_{ox}$.

For many gate oxide MOSFETs the trapped holes after hole transport and trapping are located within 50-100 $\AA$ of the silicon-silicon dioxide interface.[14] If this condition exists, then for $t_{ox} \gg 50 - 100\AA$,

$$\Delta N_{OT} \simeq \frac{\Delta V_{MG} C_{ox}}{q} \tag{35}$$

Unfortunately, many state-of-the-art hardened oxides are on the order of 200-500 $\AA$ thick. In this case, for equation (35) to be valid the trapped holes would need to be located on the order of 50 $\AA$ or less from the interface. Since hole detrapping by tunneling begins immediately after hole transport and trapping, those holes trapped within a few 10s of $\AA$ of the interface are detrapped in times comparable to the post-irradiation measurement time. Therefore, in gate oxides of <500 $\AA$, equation (35) may severely underestimate the number of trapped holes. However, since the assumption

of uniform trapping yields a value twice the value for Si-SiO_2 interface trapping, the underestimate will be less than a factor of 2.

Because most techniques applied to MOS capacitors use the same assumptions about the spatial dependence of the trapped holes, the use of equation (35) will be quite adequate for comparing ΔN_{OT} to values obtained from other techniques for thin gate oxides.

There is some evidence[15] that in thick field oxides, including bipolar recessed field oxides, the holes are uniformly trapped in the bulk. In this case,

$$\Delta N_{OT} = \frac{2\Delta V_{MG} C_{ox}}{q} \tag{36}$$

Equation (36) is also valid for irradiation at low temperature (<76° K) since, in this case, hole transport is impeded, and the holes are uniformly trapped in the bulk near where they are created.

The calculation of ΔN_{IT} is given in Section 2.3.

4.4 APPLICATION RECOMMENDATIONS.

Use of the midgap or subthreshold swing method of the subthreshold charge separation technique requires a straight line approximation to the subthreshold curve. The midgap method uses the straight line fit for extrapolation to a midgap voltage, and the subthreshold swing method uses the fit to calculate the voltage shift due to interface states. The midgap method has been more widely used by the technical community. Also, the additional assumption that $a \gg (C_D + C_{IT})/C_{ox}$ hinders the application of the subthreshold swing method to technologies which exhibit high interface state generation.

Linear fits to the subthreshold curve is complicated by nonideal subthreshold characteristics. The approach to the application of the subthreshold technique to MOSFETs with nonideal characteristics is discussed in Section 3. Once a linear fit to

a nonideal subthreshold curve is chosen, the analysis follows the approach presented in Section 4.3. The calculated voltage shifts from MOSFETs with nonideal characteristics should be combined with speculation to the cause of the nonideal characteristics. This will aid other readers in understanding the analysis.

SECTION 5

LIST OF REFERENCES

1. Schwank, J. R., et al., "Physical Mechanisms Contributing to Device 'Rebound'," *IEEE Trans. Nuc. Sci.*, NS-31, December 1984, pp. 1439.

2. Winokur, P. S., et al., "Optimizing and Controlling the Radiation Hardness of a Si-Gate CMOS Process," *IEEE Trans. Nuc. Sci.*, NS-32, December 1984, pp. 3954-3960.

3. Winokur, P. S., et al., "Correlating the Radiation Response of MOS Capacitors and Transistors," *IEEE Trans. Nuc. Sci.*, NS-31, December 1984.

4. Lenahan, P. M. and P. V. Dressendorfer, "Hole Traps and Trivalent Silicon Centers in Metal/Oxide/Silicon Devices," *Journal Appl. Physics*, 55, pp. 3495 (1984).

5. Brews, J. R., "Subthreshold Behavior of Uniformly and Nonuniformly Doped Long-Channel MOSFET," *IEEE Trans. Electron Devices*, Vol. ED-26, No. 9, pp. 1282 (September 1979).

6. Sze, S. M. Physics of Semiconductor Devices, 2nd Edition, John Wiley & Sons, New York, NY (1981).

7. Van Overstraeten, R. J., G. J. Declerck, and P. A. Muls, "Theory of the MOS Transistor in Weak Inversion-New Method to Determine the Number of Surface States," *IEEE Trans. Electron Devices*, ED-22, 282-288 (1975).

8. Galloway, K. F., M. Gaitan and T. J. Russell, "A Simple Model for Separating Interface and Oxide Charge Effects in MOS Device Characteristics," *IEEE Trans. Nuc. Sci.*, NS-31, December 1984.

9. Groeseneken, G., H. E. Maes, N. Beltran, and R. F. DeKeersmaecker, "A Reliable Approach to Charge Pumping Measurements in MOS Transistors," *IEEE Trans. Electron Devices*, ED-31, 42-53 (1984).

10. Hawkins, I. D. and A. R. Peaker, "Capacitance and Conductance Deep Level Transient Spectroscopy in Field-Effect Transistors," *Appl. Phys. Lett.*, 48(3), 20 January 1986.

11. Sun, S. C. and J. D. Plummer, "Electron Mobility in Inversion and Accumulation Layers on Thermally Oxidized Silicon Surfaces," *IEEE Trans. Electron Devices,* ED-27, 1497 (1980).

12. McWhorter, P. J. and P. S. Winokur, "Simple Technique for Separating the Effects of Interface Traps and Trapped Oxide Charge in MOS Transistors," *Applied Physics Letters,* 48, 133-135 (1986).

13. Brews, J. R., "A Charge-Sheet Model of the MOSFET," *Solid State Electronics,* 21, 345 (1978).

14. Oldham, T. R., A. J. Lelis and F. B. McLean, "Spacial Distribution of Trapped Holes Determined from Tunneling Analysis and Measured Annealing," *IEEE Trans. Nuc. Sci.,* NS-33, December 1986.

15. Boesch, H. E., Jr. and F. B. McLean, "Hole Transport and Trapping in Field Oxides," *IEEE Trans. Nuc. Sci.,* NS-32, December 1985.

16. Terman, L. M., "An Investigation of Surface States of a Silicon/Silicon Dioxide Interface Employing Metal-Oxide-Silicon Diodes," *Solid State Electronics,* 5, pp. 285 (1962).

17. Brews, J. R., "Carrier-Density Fluctuations and IGET Mobility Near Threshold," *Journal of Applied Physics,* Vol. 46, No. 5, May 1975, pp. 2193-2203.

18. Saks, N. S. and M. G. Anacona, "Generation of Interface States by Ionizing Radiation at 80 K Measured by Charge Pumping and Subthreshold Slope Techniques," *IEEE Trans. Nuc. Sci.,* NS-34, December 1987, pp. 1348-1354.

19. Freitag, R. K., C. M. Dozier, and D. B. Brown, "Growth and Annealing of Trapped Holes and Interface States Using Time-Dependent Biases," *IEEE Trans. Nuc. Sci.,* NS-34, December 1987, pp. 1172-1177.

20. Lelis, A. J., et al., "Revisibility of Trapped Hole Annealing," *IEEE Trans. Nuc. Sci.*, NS-35, December 1988, pp. 1186.

21. Shanfield, Z., et al., "A New MOS Radiation-Induced Charge: Negative Fixed Interface Charge," *Journal of Radiation Effects,* Vol. 7, July 1989, to be published.

22. McWhorter, P. J., P. S. Winokur, and R. A. Pastorek, "Donor/Acceptor Nature of Radiation Induced Interface Traps," *IEEE Trans. Nuc. Sci.*, NS-35, December 1988, pp. 1154.

23. Shanfield, Z. and M. M. Moriwaki, "Critical Evaluation of the Midgap Voltage Shift Method for Determining Oxide Trapped Charge in Irradiated MOS Devices," *IEEE Trans. Nuc. Sci.*, NS-34, December 1987, pp. 1159.

APPENDIX

RECOMMENDED TEST PROCEDURE FOR SEPARATING ΔV_{OT} AND ΔV_{IT} FROM ΔV_{TH} IN IRRADIATED MOSFETS USING SUBTHRESHOLD

MIL-STD-883
TEST METHOD 10XX

Subthreshold Technique for separation of ionization induced MOSFET threshold voltage shifts into voltage components resulting from oxide trapped charge and interface states.

A.1 PURPOSE.

The purpose of this test method is to separate the ionization induced threshold voltage shift, ΔV_{TH}, in an MOS transistor into components resulting from oxide trapped charge, ΔV_{OT}, and irradiation induced interface traps, ΔV_{IT}. The technique used in this test method is based on the pre- and post-irradiation electrical characteristics in the subthreshold region.

A.1.1 Definitions.

a. **Threshold Voltage, V_{TH}.** The value of gate to source voltage extrapolated to a drain current, I_D, of zero using a plot of I_D or $\sqrt{I_D}$, versus gate to source voltage, V_{GS}. For linear region operation, I_D, is extrapolated and for saturated operation, $\sqrt{I_D}$ is extrapolated.

b. **Radiation Induced Threshold Voltage Shift, ΔV_{TH}.** The post-irradiation value of V_{TH} minus the pre-irradiation value. ΔV_{TH}, can be either positive or

negative depending on whether the net radiation induced charge is negative or positive, respectively.

c. **Inversion Voltage, V_{INV}.** The gate to source voltage corresponding to a surface potential of $2\phi_B$, where ϕ_B is the bulk Fermi potential.

d. **Radiation Induced Inversion Voltage Shift, ΔV_{INV}.** The post-irradiation value of V_{INV} minus the pre-irradiation value.

e. **Inversion Current, I_{INV}.** The value of drain current at a surface potential of $2\phi_B$.

f. **Midgap Voltage, V_{MG}.** The gate to source voltage for a surface potential of ϕ_B.

g. **Radiation Induced Midgap Voltage Shift, ΔV_{MG}.** The post-irradiation value of V_{MG} minus the pre-irradiation value.

h. **Midgap Current, I_{MG}.** The value of drain current at a surface potential of ϕ_B.

i. **Surface Potential, ϕ_S.** The potential at the semiconductor surface measured with respect to the intrinsic Fermi level. For the flat band condition, $\phi_S = 0$.

j. **Bulk Fermi Potential, ϕ_B.** The surface potential at which the Fermi level and the intrinsic Fermi level coincide.

k. **Transconductance, G_M.** The rate of change in I_D with respect to source to gate voltage at a constant source to drain voltage. For an ideal MOSFET in the linear region, $G_M = (Z/L_{eff})\,\mu C_{oz} V_D$, where Z is the channel width, L_{eff} the effective channel length, μ the mobility, C_{oz} the oxide capacitance per unit area and V_D the drain voltage.

l. **Oxide Thickness, t_{oz}.** The thickness of the gate oxide measured from the gate-SiO_2 interface to the Si-SiO_2 interface.

m. **Channel Doping Density, N_D, N_A.** The donor (P-type) or acceptor (N-type) concentration in the channel region adjacent to the gate oxide-silicon interface.

n. **Subthreshold.** $\phi_B \leq \phi_S < 2\phi_B$, also referred to as weak inversion.

o. **Subthreshold Swing, S.** The subthreshold swing is the reciprocal of the subthreshold slope of log I_D versus V_{GS}. S is measured in units of volts per decade.

A.2 APPARATUS.

A.2.1 Instrumentation.

To measure the subthreshold drain current versus the gate to source voltage on standard microcircuit MOSFETS, the instrumentation required consists of, as a minimum, two voltage sources and four ammeters with the following characteristics.

Equipment	Requirements
Drain-Source Power Supply	±10 V, 0.01 V resolution
Gate-Source Power Supply	±10 V, 0.001 V resolution
Ammeters for measuring	±1 pA minimum resolution
terminal currents	±10 mA maximum range

If the MOSFETs under test (MUTs) are power MOS, parasitic field oxide structures or higher voltage linear MOSFETs, the maximum voltage requirements will be much higher. For example, parasitic field oxide transistors, FOXFETs, may have initial threshold voltages of several hundred volts.

In most applications of the charge separation technique the subthreshold drain current versus gate-source voltage characteristic will be measured with a programmable tester with the proper current and voltage capabilities. The most widely used instrument for MOSFET subthreshold I-V measurements is the HP4145 parameter analyzer. The basic system has a 100 V, 100 mA capability with 1 mV, 1 pA resolution. For rapid subthreshold I-V measurements, a programmable tester, the Transient Annealing Test System (TATS) has been developed by Design Engineering, Inc. (DEI), of Albuquerque, NM. This instrument is current programmable and is capable of 100 pA measurements in 200 μs and >100 nA measurements in 70 μs. The subthreshold I-V measurements can be made with any instrument having the appropriate characteristics.

A.2.2 Temperature Control.

The subthreshold drain current varies as the exponential of $\left(\frac{q\phi_B}{kT}\right)$. Therefore, the temperature of the measurement should be controlled to within a few °C, since the charge extraction requires a comparison of pre-irradiation and post-irradiation data. For many applications, the charge separation will be performed at a temperature other than room ambient. For these measurements, special heating and/or cooling apparatus are required. The heating/cooling apparatus shall be capable of controlling the MUT temperature to within ±2°C. A temperature sensing device shall be provided which shall be in thermal contact with the MUT. The readout shall be capable of 0.5 C resolution and calibrated to ±1°C accuracy. The temperature control apparatus shall allow for power and sense leads to the MUT and shall not degrade the drain current measurement by more than 10 pA.

A.3 PROCEDURE.

A.3.1 Device Identification

In all cases, each MUT shall be individually identified (marked with a permanent marking) and its identification shall be included in all pre- and post-irradiation data.

A.3.2 Initial Characterization.

Using the appropriate test apparatus, the MUT shall be characterized using the test configuration illustrated in Figure 23. The gate-source voltage shall be swept from accumulation to inversion in order to clearly identify the leakage, subthreshold, and inversion regions. The drain voltage may be selected for either linear or saturated operation. It is recommended that measurements be made in the linear region with V_D between 100 mV and 150 mV. As the gate-source voltage is stepped from leakage (accumulation) through inversion, all four currents, I_G, I_S, I_D and I_B shall

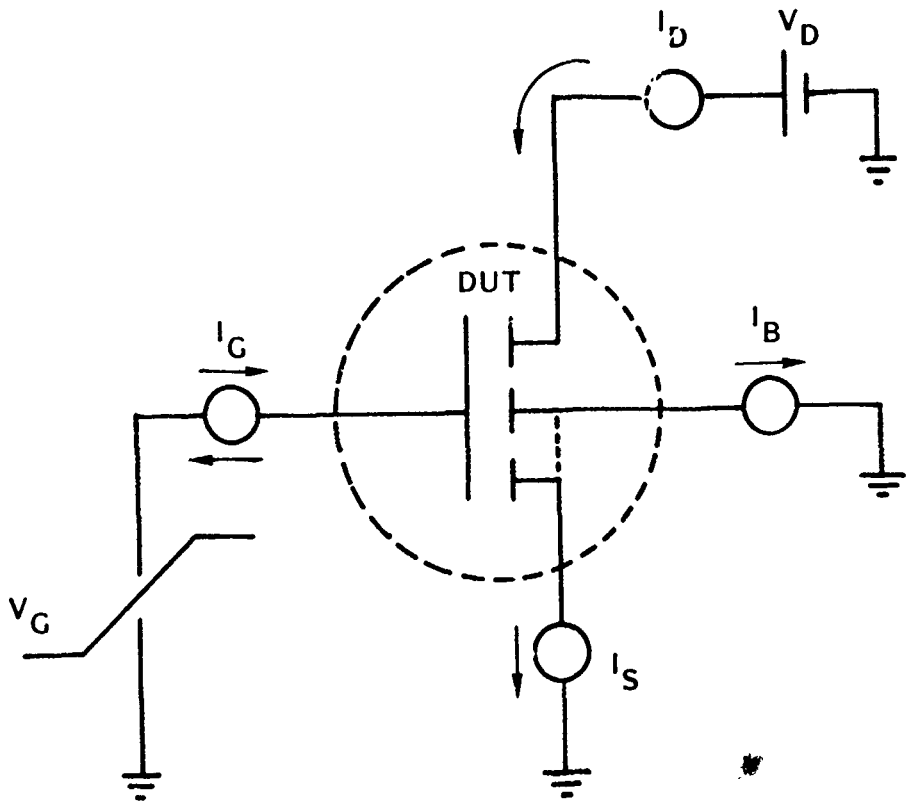

Figure 23. Test configuration for measurement of $I_D(I_S)$ versus V_G.

be monitored. If there is no access to the body (channel, substrate) then only three currents shall be monitored. In some devices (SOS, SOI), the body floats and in some devices (power MOS) the source and body are internally tied together. Once all of the available terminal currents are measured, a plot is made of log I versus V_{GS}. All three or four currents should be plotted on the same graph for comparison.

The purpose of plotting all currents is to analyze the MUT for leakage paths and parasitics to determine the idealty of the subthreshold characteristic. Discussion of nonideal behavior is given in the guideline document. Distortions of the subthreshold characteristic may be caused by gate leakage, body-drain or body-source leakage, or parasitics. After pre-irradiation characterization, it may be decided that the part is unacceptable for charge separation studies or that the source current rather than drain current is a better representation of the ideal channel current.

An example of a near ideal subthreshold characteristic is shown in Figure 24 for an n-channel transistor. For this example, the leakages are all small and the source or drain current could be used for charge separation.

Based on the initial characterization, a decision must be made as to the suitability of the test sample for charge separation. For those samples deemed suitable, a decision is made whether to measure drain current, I_D or source current, I_S. If both I_D and I_S are suitable, then the decision may be based on convenience.

A.4 PRE-/POST-IRRADIATION CHARACTERIZATION.

A.4.1 Pre-Irradiation Characterization.

Because of the sensitivity of $I_{D(S)}$ to temperature, the pre-irradiation characterization used for charge separation should be made either in a temperature controlled chamber or immediately prior to irradiation. The drain (or source) current is measured from accumulation (or leakage) through the subthreshold region and well into inversion at a fixed value of drain to source voltage (V_{DS}). For linear measurements,

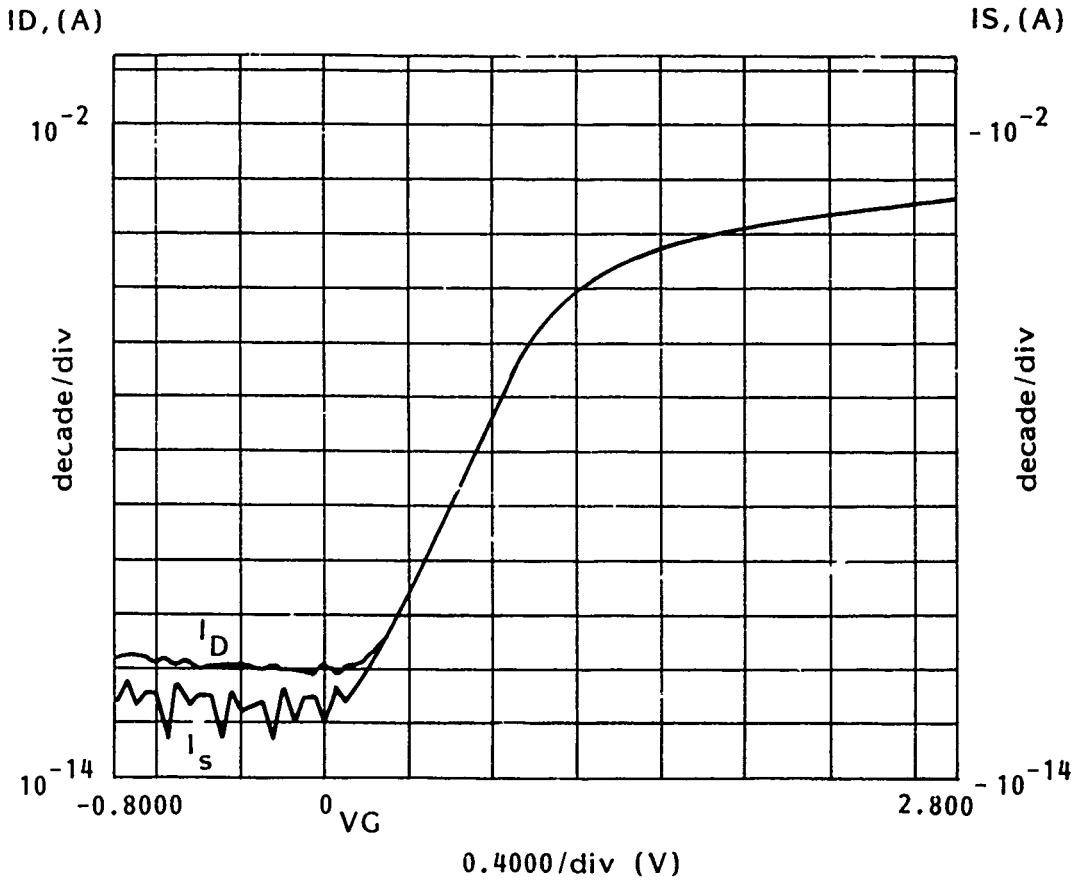

Figure 24. Near ideal subthreshold characteristics from an n-channel transistor.

V_{DS} should be chosen between 100 and 150 mV. For saturated operation, the value of V_{DS} will depend on the threshold voltage and the rated value of V_{DS}. If the test samples are conventional CMOS microcircuit MOSFETs and saturated measurements are specified, then V_{DS} can be set at the nominal power supply voltage.

If the measuring instrument is automatically stepped through programmed values of V_{GS}, the step size shall be adjusted so that a minimum of 3 $I_{D(S)}$ values per decade current are measured in subthreshold. Also, the dwell time at a fixed V_{GS} shall be adjusted to assure adequate settling time. If an HP4145 or similar instrument is used, the medium or long measurement time setting should be used.

The value of $I_{D(S)}$ for each value of V_{GS} shall be recorded, along with the part identification number, date and time, temperature and a notation for pre-irradiation.

A.4.1.1 In-Source and In-Situ Test Setup. If the MUT is being measured in-source (i.e., while it is being irradiated), or in-situ (i.e., in the irradiation test fixture but not while it is being irradiated), the test fixture and cabling connecting the test instrument must be designed for low current measurements. In addition, the test fixture must provide a mechanism for switching the MUT from the irradiation and/or annealing bias conditions to the measurement mode. In order to obtain accurate measurements in the subthreshold region, the leakage and noise currents in the test fixture and cabling must be less than 10 pA. Therefore, measurement cables should be shielded and of minimum length. The leakage and noise currents shall be measured in the test setup by monitoring the $I_{D(S)}$ versus V_{GS} characteristic with no device in the socket. Maximum current over the voltage range of interest should not exceed 10 pA.

A.4.1.2 In-Source, In-Situ, and Post-Irradiation Measurements. The "post" irradiation characterization may be performed in-source, in-situ, or at a test setup away from the radiation source. The details of performing the irradiation are provided in MIL-STD-883 test method 1019.3 and MIL-HDBK-279, "Piecepart Total Dose Hardness Assurance Guideline." The test procedure for measuring the $I_{D(S)}$

versus V_{GS} characteristic is the same for post-irradiation as for pre-irradiation with the following cautions. First, the range of the V_{GS} sweep to go from leakage through inversion will change for two reasons: a) hole trapping in the oxide will cause the entire curve to shift toward negative values, and b) interface states will cause a stretchout of the subthreshold region. Therefore, the range of V_{GS} values will have to be adjusted to assure that the entire $I_{D(S)}$ versus V_{GS} characteristic is measured. The second caution concerns the measurement duty cycle for in-source measurements. During the $I_{D(S)}$ versus V_{GS} measurement cycle, the gate voltage is usually being swept from negative to positive values (for n-channel device or positive to negative for a p-channel). Since the ionization response is dependent on the oxide electric field magnitude and direction during irradiation, the time period of the measurement must be minimized. The restrictions on measurement time will depend on dose rate, the dose values selected for measurement, and the total number of test samples being measured. The duty cycle should be maintained at <1%.

The third caution concerns temperature. If the test sample temperature is not controlled by a heating or cooling stage, the temperature will increase as a result of the irradiation. If the measurements are in-situ, either the dose rate must be kept low enough to cause an insignificant temperature increase in the MUT, or the radiation source and MUT must be cooled with forced air or nitrogen. For in-situ measurements, either the radiation source and MUT should be cooled, or the MUT should be allowed to cool prior to characterization when the source is removed.

With each set of measurements, the individual $I_{D(S)}, V_{GS}$ data points shall be recorded along with the part identification number, temperature dose rate, dose and time between end of irradiation and initiation of test.

A.4.2 Data Analysis.

A.4.2.1 Determination of V_{TH} and ΔV_{TH}. V_{TH} shall be determined using an extrapolation of the drain (or source) current versus the gate-source voltage. If measurements were made using $V_{DS} = 100 - 150mV$ (linear operation), a plot of $I_{D(S)}$

versus V_{GS} shall be made. The straight line portion of $I_{D(S)}$ shall be extrapolated to $I_{D(S)} = 0$. V_{TH} is the V_{GS} intercept of this extrapolation. If the value of V_{DS} was chosen for saturated operation then a plot of $\sqrt{I_{D(S)}}$ versus V_{GS} shall be made. Again, the straight line portion of $\sqrt{I_{D(S)}}$ shall be extrapolated $I_{D(S)} = 0$. V_{TH} is the V_{GS} intercept with this extrapolation.

The value of ΔV_{TH} is found from the following relation,

$$\Delta V_{TH} = V_{TH\gamma} - V_{THI}$$

where $V_{TH\gamma}$ is found from the post-irradiation I_D versus V_{GS} characteristic, and V_{THI} is found from the pre-irradiation characteristic.

A.4.2.2 Calculation of I_{MG} and I_{INV}. The values of midgap current I_{MG} and inversion current I_{INV} are found from the following equations.

$$I_{MG} = \frac{G_M}{V_{DS}} \frac{a}{2\beta^2} \left(\frac{n_i}{N}\right)^2 \frac{e^{\beta\phi_B}}{(\beta\phi_B - 1)^{1/2}} \qquad V_{DS} \gg \frac{kT}{q}$$

$$I_{INV} = \frac{G_M}{V_{DS}} \frac{a}{2\beta^2} \left(\frac{n_i}{N}\right)^2 \frac{e^{2\beta\phi_B}}{(2\beta\phi_B - 1)^{1/2}} \qquad V_{DS} \gg \frac{kT}{q}$$

where

$$\frac{G_M}{V_{DS}} = \frac{Z\mu C_{ox}}{L_{eff}}$$

$$a = \frac{\sqrt{2}\varepsilon_s}{C_{ox} L_d}$$

$$L_d = \left(\frac{kT\varepsilon_s}{Nq^2}\right)^{1/2}$$

$$\phi_B = \frac{kT}{q} \ell n \left(\frac{N}{n_i}\right)$$

$$\beta = \frac{q}{kT}$$

N = silicon doping density at SiO_2 - Si interface

n_i = intrinsic carrier concentration

ε_s = silicon dielectric constant

C_{ox} = oxide capacitance per unit area

$C_{ox} = \frac{\varepsilon_{ox}}{t_{ox}}$

ε_{ox} = oxide (insulator) dielectric constant

t_{ox} = oxide thickness

Z = channel width

L_{eff} = effective channel length

μ = channel mobility

In order to calculate I_{MG} and I_{INV}, it is necessary to determine the quantities N, t_{ox} and G_M/V_{DS}. Table 1 is a list of methods for determining these parameters.

Table 1. Parameter required for calculation.

Parameter	Method of Determination
N	a) V_{TH} versus substrate bias. b) Process code calculation (e.g., SUPREM). c) Spreading resistance profiles.
t_{ox}	a) Ellipsometry. b) C-V Measurements. c) Interferometry.
$\frac{G_M}{V_{DS}}$	a) Plot of $\Delta I_D/\Delta V_{GS}$.

The quantities N and t_{ox} are normally determined by the manufacturer and should be requested for each sample type and lot. The value of G_M/V_{DS} is obtained from the inversion data of $I_{D(S)}$ versus V_{GS}. A plot of $\Delta I_{D(S)}/\Delta V_{GS}$ versus V_{GS} is made such as the one shown in Figure 25. The value of G_M used in the calculation should be the maximum value of G_M which occurs near the threshold voltage.

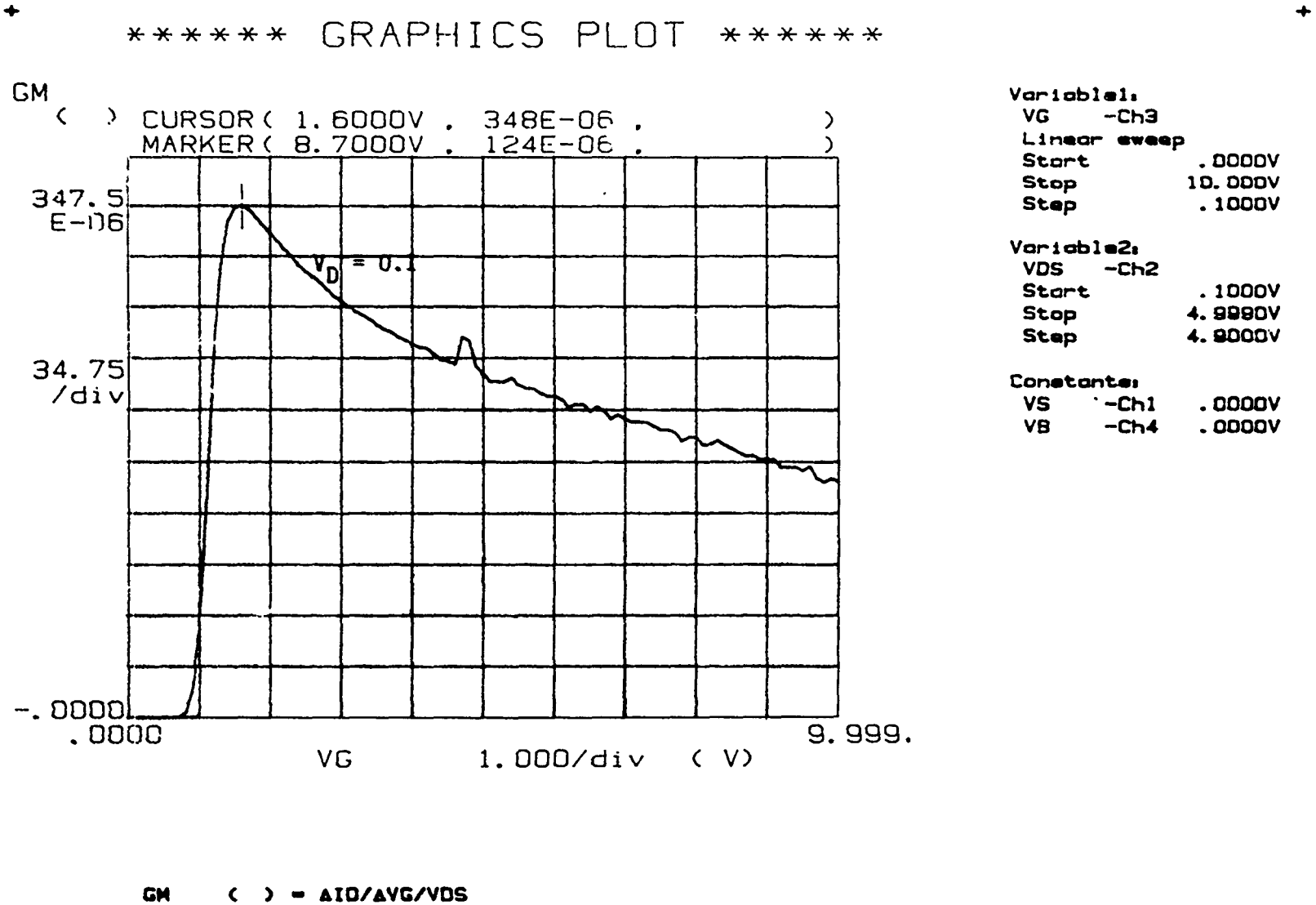

Figure 25. Plot of G_M versus gate voltage in the linear region for drain voltage of 0.1.

Once the values of N, t_{ox}, and G_M/V_{DS} are obtained for each MUT, the values of I_{MG} and I_{INV} can be calculated. The pre-irradiation value of I_{MG} and I_{INV} should be used for all calculations involving these terms. The rationale for this is discussed in the guidelines.

A.4.3 Determination of V_{INV} and ΔV_{INV}.

The inversion voltage, V_{INV}, is defined as the value of gate to source voltage corresponding to the calculated value of I_{INV}. The value of V_{INV} is found from a plot of log $I_{D(S)}$ versus V_{GS} by interpolating between the two closest measurements on either side of I_{INV}. A logarithmic interpolation is preferred. The value of ΔV_{INV} is given by the relation

$$\Delta V_{INV} = V_{INV_1} - V_{INVI}$$

where V_{INV_1} is the post-irradiation value of V_{INV} and V_{INVI} is the pre-irradiation value.

A.4.4 Determination of ΔV_{MG} and ΔS.

In order to apply the subthreshold charge separation technique, it is necessary to determine ΔV_{MG} and/or ΔS from the pre- and post-irradiation subthreshold characteristics. ΔV_{MG} is the difference between the post-irradiation value of the midgap voltage, V_{MG_1}, and the pre-irradiation value, V_{MGI}. The values of V_{MGI} and V_{MG_1} are found from a plot of log $I_{D(S)}$ versus V_{GS} for the pre- and post-irradiation data set of $I_{D(S)}, V_{GS}$ points. A typical set of pre- and post-irradiation curves are shown in Figure 26. The straight line portion of the subthreshold log $I_{D(S)}$ versus V_{GS} curve is extrapolated to the calculated value of I_{MG}. The value of V_{GS} at I_{MG} is the value of V_{MG}. For each post-irradiation data set

$$\Delta V_{MG} = V_{MG_1} - V_{MGI}.$$

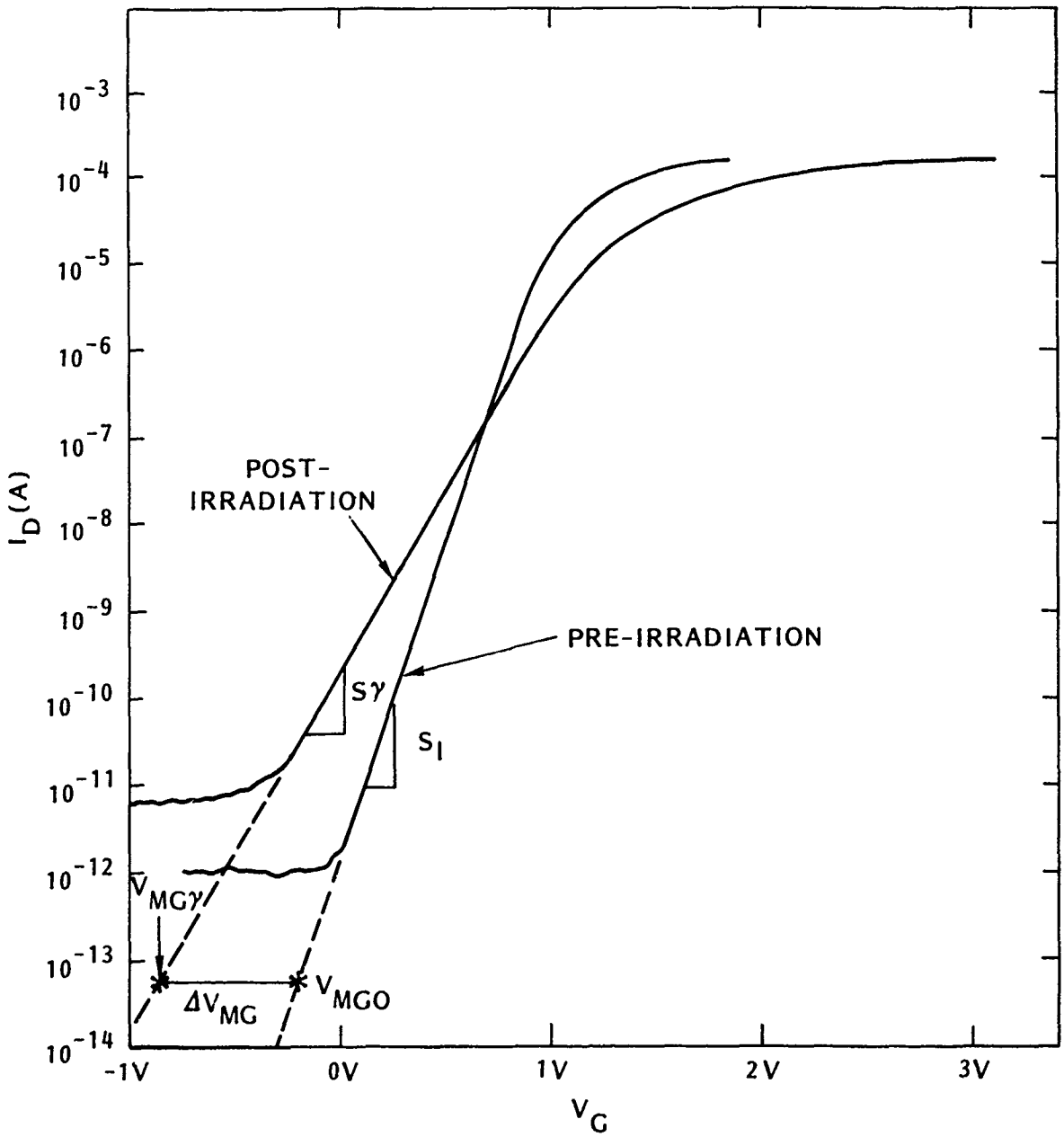

Figure 26. Determination of pre- and post-irradiation subthreshold swings S_I and S_γ, respectively.

The subthreshold swing, ΔS, is equal to the post-irradiation value of the subthreshold swing, S_γ, minus the pre-irradiation value S_I. The values of S_I and S_γ are found from the same straight lines used to extrapolated to the values of V_{MGI} and $V_{MG\gamma}$ as shown in Figure 26. The values S_I and S_γ are measured in volts per decade of current.

A.4.5 Separation of ΔV_{TH} or ΔV_{INV} into ΔV_{OT} and ΔV_{IT}.

The charge separation technique can be applied to either the threshold voltage shift, ΔV_{TH}, or the inversion voltage shift, ΔV_{INV}. ΔV_{TH} is often preferred since it is the parameter typically specified and measured as a performance parameter. However, ΔV_{INV} has greater physical significance since it is well defined in terms of the surface potential. Although either parameter may be used for charge separation, ΔV_{TH} is usually preferred for engineering applications.

A.4.5.1 Method A: Midgap Voltage Techniques. In the midgap voltage technique the value of ΔV_{OT}, the voltage component due to oxide trapped charge, is found from the value of midgap voltage shift,

$$\Delta V_{OT} = \Delta V_{MG} = V_{GM\gamma} - V_{MGI}$$

The value of ΔV_{IT}, the voltage component due to interface states, is then equal to the difference between $\Delta V_{TH}(\Delta V_{INV})$ and ΔV_{OT}, i.e.,

$$\Delta V_{IT} = \Delta V_{TH}\left(\Delta V_{INV}\right) - \Delta V_{OT}$$

A.4.5.2 Method B: Subthreshold Swing Technique. In the subthreshold swing technique, the value of ΔV_{IT} is found from the value of ΔS according to the following relation

$$\Delta V_{IT} = \left(\frac{q\phi_B}{kT\ell n10}\right)\Delta S$$

where $\Delta S = S_\gamma - S_I$ and $\phi_B = kT/q\ell n(N/n_i)$. The value of ΔV_{OT} is then found from $\Delta V_{TH}(\Delta V_{INV})$ according to the relation

$$\Delta V_{OT} = \Delta V_{TH}\left(\Delta V_{INV}\right) - \Delta V_{IT}$$

A.5 REPORTING.

Charge separation reporting shall, at a minimum, include the following information: a) part identification; b) irradiation data including dose rate, dose levels, irradiation bias, anneal bias, time between irradiation and test, test type (in-source, in-situ or pre/post) and test temperature; c) values of N and t_{ox} used in the calculations; d) whether I_D or I_S was used; e) V_{DS}; f) whether ΔV_{TH} or ΔV_{INV} was used; g) data separation method (A or B); and h) calculated values of ΔV_{OT} and ΔV_{IT} at each dose.

A.6 SUMMARY.

The following details shall be specified in the applicable procurement document.

1. Part types and quantities to be tested.
2. Test temperature.
3. Test instruments if other than specified in A.2.1.
4. Irradiation test methods, dose rate, dose levels, irradiation and anneal biases, and measurement times.
5. V_{DS} for linear or saturated measurement.
6. Charge separation method A or B.
7. Whether ΔV_{TH} or ΔV_{INV} is used for charge separation.

DISTRIBUTION LIST

DNA-TR-89-157

DEPARTMENT OF DEFENSE

ASSISTANT TO THE SECRETARY OF DEFENSE
ATOMIC ENERGY
ATTN: EXECUTIVE ASSISTANT

DEFENSE ADVANCED RSCH PROJ AGENCY
ATTN: ASST DIR/ELCTRNIC SCI DIV
ATTN. R REYNOLDS

EFENSE ELECTRONIC SUPPLY CENTER
ATTN: DEFC-EAA

DEFENSE INTELLIGENCE AGENCY
ATTN: DT-1B
ATTN: RTS-2B

DEFENSE LOGISTICS AGENCY
ATTN: DLA-QEL

DEFENSE NUCLEAR AGENCY
3 CYS ATTN: RAEE (TREE)
4 CYS ATTN: TITL

DEFENSE NUCLEAR AGENCY
ATTN: TDNM
ATTN: TDTT
2 CYS ATTN: TDTT W SUMMA

DEFENSE TECHNICAL INFORMATION CENTER
2 CYS ATTN: DTIC/FDAB

DNA PACOM LIAISON OFFICE
ATTN: DNALO

FIELD COMMAND DEFENSE NUCLEAR AGENCY
ATTN: FCPF R ROBINSON

JOINT DATA SYSTEM SUPPORT CTR
ATTN: C-312
ATTN: C-330

JOINT STRAT TGT PLANNING STAFF
ATTN: JKC (ATTN: DNA REP)
ATTN: JKCS
ATTN: JPEM

STRATEGIC AND THEATER NUCLEAR FORCES
ATTN: DR E SEVIN

DEPARTMENT OF THE ARMY

HARRY DIAMOND LABORATORIES
ATTN: SLCHD-NW-EC
ATTN: SLCHD-NW-EC J MILETTA
ATTN: SLCHD-NW-RA
ATTN: SLCHD-NW-RC
ATTN: SLCHD-NW-RP
ATTN: SLCHD-NW-RP F MCLEAN
ATTN: SLCHD-NW-TS
ATTN: W PATTERSON

U S ARMY GARRISON
ATTN: LIBRARY

U S ARMY MISSILE COMMAND
ATTN: AMCPM-HA-SE-MS

U S ARMY MISSILE COMMAND/AMSMI-RD-CS-R
ATTN: AMSMI-RD-CS-R (DOCS)

U S ARMY NUCLEAR & CHEMICAL AGENCY
ATTN: MONA-NU

U S ARMY RESEARCH OFFICE
ATTN: R GRIFFITH

U S ARMY STRATEGIC DEFENSE CMD
ATTN: BMDSC-AV J HARPER
ATTN: CSSD-H-SAV

U S ARMY STRATEGIC DEFENSE COMMAND
ATTN: CSSD-SL

U S ARMY WHITE SANDS MISSILE RANGE
ATTN: STEWS-TE-AN A DE LA PAZ
ATTN: STEWS-TE-AN J MEASON
ATTN: STEWS-TE-N K CUMMINGS
ATTN: STEWS-TE-N T ARELLANES

DEPARTMENT OF THE NAVY

NAVAL AIR SYSTEMS COMMAND
ATTN: AIR 931A

NAVAL ELECTRONICS ENGRG ACTVY, PACIFIC
ATTN: CODE 250 D OBRYHIM

NAVAL POSTGRADUATE SCHOOL
ATTN: CODE 1424 LIBRARY

NAVAL RESEARCH LABORATORY
ATTN: CODE 4040 J BORIS
ATTN: CODE 4600 D NAGEL
ATTN: CODE 4610 J RITTER
ATTN: CODE 4611 E PETERSON
ATTN: CODE 4612 D WALKER
ATTN: CODE 4613 A B CAMPBELL
ATTN: CODE 4614 L AUGUST
ATTN: CODE 4652 G MUELLER
ATTN: CODE 4653 A NAMENSON
ATTN: CODE 4673 A KNUDSON
ATTN: CODE 4682 C DOZIER
ATTN: CODE 4682 D BROWN
ATTN: CODE 5813 N SAKS
ATTN: CODE 5814 D MCCARTHY
ATTN: CODE 5816 R HEVEY
ATTN: CODE 5816 R LAMBERT
ATTN: CODE 6804 M PECKERAR
ATTN: CODE 6810 J KILLIANY
ATTN: CODE 6816 E D RICHMOND
ATTN: CODE 6816 H HUGHES
ATTN: CODE 6816 W JENKINS

NAVAL SEA SYSTEMS COMMAND
ATTN: CODE 08K NEWHOUSE

NAVAL SURFACE WARFARE CENTER
ATTN: CODE H21 F WARNOCK
ATTN: CODE H23 R SMITH

NAVAL SURFACE WARFARE CENTER
ATTN: CODE H-21

NAVAL TECHNICAL INTELLIGENCE CTR
ATTN: NISC LIBRARY

NAVAL UNDERWATER SYS CENTER
ATTN: 8092

NAVAL WEAPONS EVALUATION FACILITY
ATTN: CLASSIFIED LIBRARY

NAVAL WEAPONS SUPPORT CENTER
ATTN: CODE 6054 D PLATTETER

OFC OF THE DEP ASST SEC OF THE NAVY
ATTN: L J ABELLA

OFFICE OF CHIEF OF NAVAL OPERATIONS
ATTN: NOP 985F

DEPARTMENT OF THE AIR FORCE

AERONAUTICAL SYSTEMS DIVISION
ATTN: ASD/ENSS

AIR FORCE CTR FOR STUDIES & ANALYSIS
2 CYS ATTN: AFCSA/SAMI (R GRIFFIN)

AIR UNIVERSITY LIBRARY
ATTN: AUL-LSE

OGDEN AIR LOGISTICS COMMAND
ATTN: OO-ALC/MMEDD/HARDNESS CNTRL
ATTN: OO-ALC/MMGR/DOCUMENT CNTRL

ROME AIR DEVELOPMENT CENTER, AFSC
ATTN: RBR J BRAUER

ROME AIR DEVELOPMENT CENTER, AFSC
ATTN: ESR

SPACE DIVISION/YA
ATTN: YAS

SPACE DIVISION/YAR
ATTN: YAR CAPT STAPANIAN

SPACE DIVISION/YD
ATTN: YD

SPACE DIVISION/YE
ATTN: YE

STRATEGIC AIR COMMAND/XRFS
ATTN: XRFS

WEAPONS LABORATORY
ATTN: NTAAB C BAUM
ATTN: NTC M SCHNEIDER
ATTN: NTCAS
ATTN: NTCAS J MULLIS
ATTN: NTCER R MAIER
ATTN: NTCOX/W KEMP
ATTN: NTCT MAJ HUNT
ATTN: NTCTD
ATTN: SUL
ATTN: TAS MAJ SQUILLER

WRIGHT RESEARCH & DEVELOPMENT CENTER
ATTN: AFWAL/ELE
ATTN: AFWAL/MLTE

3416TH TECHNICAL TRAINING SQUADRON (ATC)
ATTN: TTV

DEPARTMENT OF ENERGY

DEPARTMENT OF ENERGY
ATTN: ESHD

LAWRENCE LIVERMORE NATIONAL LAB
ATTN: D MEEKER
ATTN: J YEE
ATTN: H KRUGER
ATTN: W ORVIS

LOS ALAMOS NATIONAL LABORATORY
ATTN: E LEONARD

SANDIA NATIONAL LABORATORIES
ATTN: ORG 2100 H SAXTON
ATTN: ORG 2126 J E GOVER
ATTN: ORG 2144 P V DRESSENDORFER
ATTN: ORG 2146 T A DELLIN
ATTN: ORG 2321 L D POSEY
ATTN: ORG 7200 J A HOOD
ATTN: T F WROBEL

OTHER GOVERNMENT

CENTRAL INTELLIGENCE AGENCY
ATTN: OSWR/NED
ATTN: OSWR/STD/MTB

DEPARTMENT OF TRANSPORTATION
ATTN: ARD-350

NASA
ATTN: CODE 313 V DANCHENKO
ATTN: CODE 600 E STASSINOPOULOS
ATTN: CODE 660 J TRAINOR
ATTN: CODE 724.1 M JHABVALA

NATIONAL INSTITUTE OF STANDARDS & TECHNOLOGY
ATTN: CODE A347 J MAYO-WELLS
ATTN: CODE A353 S CHAPPELL
ATTN: P ROITMAN

DEPARTMENT OF DEFENSE CONTRACTORS

ADVANCED RESEARCH & APPLICATIONS CORP
ATTN: L PALKUTI
ATTN: R ARMISTEAD

AEROJET ELECTRO-SYSTEMS CO
ATTN: D TOOMB

AEROSPACE CORP
ATTN: A AMRAM
ATTN: C RICE
ATTN: D FRESH
ATTN: D SCHMUNK
ATTN: I GARFUNKEL
ATTN: J REINHEIMER
ATTN: J B BLAKE
ATTN: K G HOLDEN

ATTN: M DAUGHERTY
ATTN: M HOPKINS
ATTN: N SRAMEK
ATTN: P BUCHMAN
ATTN: R SLAUGHTER
ATTN: W A KOLASINSKI

ALLIED-SIGNAL, INC
ATTN: DOCUMENT CONTROL

AMPEX CORP
ATTN: B RICKARD
ATTN: K WRIGHT

ANALYTIC SERVICES, INC (ANSER)
ATTN: A HERNDON
ATTN: A SHOSTAK

BDM INTERNATIONAL INC
ATTN: C M STICKLEY

BDM INTERNATIONAL INC
ATTN: D WUNSCH

BOEING CO
ATTN: A JOHNSTON
ATTN: M ANAYA
ATTN: C ROSENBERG
ATTN: D EGELKROUT
ATTN: E L SMITH
ATTN: I ARIMURA
ATTN: R CALDWELL
ATTN: W DOHERTY
ATTN: O MULKEY

CALIFORNIA INSTITUTE OF TECHNOLOGY
ATTN: C BARNES

CALSPAN CORP
ATTN: R THOMPSON

CHARLES STARK DRAPER LAB, INC
ATTN: J BOYLE
ATTN: N TIBBETTS
ATTN: P GREIFF
ATTN: W D CALLENDER

CINCINNATI ELECTRONICS CORP
ATTN: L HAMMOND

CLEMSON UNIVERSITY
ATTN: P J MCNULTY

COMPUTER SCIENCES CORP
ATTN: A SCHIFF

DAVID SARNOFF RESEARCH CENTER, INC
ATTN: R SMELTZER

E-SYSTEMS, INC
ATTN: K REIS

EATON CORP
ATTN: R BRYANT

ELECTRONIC INDUSTRIES ASSOCIATION
ATTN: J KINN

FORD AEROSPACE CORPORATION
ATTN: TECHNICAL INFORMATION SRVS

GENERAL ELECTRIC CO
ATTN: D EDELMAN
ATTN: D TASCA
ATTN: DOCUMENTS LIBRARY
ATTN: H ODONNELL
ATTN: J ANDREWS
ATTN: R BENEDICT
ATTN: TECHNICAL LIBRARY

GENERAL ELECTRIC CO
ATTN: B FLAHERTY
ATTN: G BENDER
ATTN: L HAUGE

GENERAL ELECTRIC CO
ATTN: G GATI

GENERAL ELECTRIC CO
ATTN: D NERAD

GENERAL ELECTRIC CO
ATTN: J MILLER
ATTN: P HEILAND

GENERAL RESEARCH CORP
ATTN: A HUNT

GEORGE WASHINGTON UNIVERSITY
ATTN: A FRIEDMAN

GRUMMAN AEROSPACE CORP
ATTN: J ROGERS

GTE GOVERNMENT SYSTEMS CORPORATION
ATTN: GEORGE COWEN

H. M. WEIL CONSULTANTS, INC
ATTN: H WEIL

HARRIS CORP
ATTN: J C LEE
ATTN: J W SWONGER

HARRIS CORPORATION
ATTN: E YOST
ATTN: W ABARE

HONEYWELL INC
ATTN: R JULKOWSKI

HONEYWELL, INC
ATTN: MS 725-5

HONEYWELL, INC
ATTN: R BELT

HUGHES AIRCRAFT CO
ATTN: W SCHENET

HUGHES AIRCRAFT COMPANY
ATTN: E KUBO
ATTN: L DARDA

IBM CORP
ATTN: H MATHERS

IBM CORP
ATTN: J ZIEGLER

IBM CORP
ATTN: N HADDAD

IIT RESEARCH INSTITUTE
ATTN: I MINDEL

INSTITUTE FOR DEFENSE ANALYSES
ATTN: TECH INFO SERVICES

IRT CORP
ATTN: MDC

JAYCOR
ATTN: M TREADAWAY
ATTN: R STAHL

JAYCOR
ATTN: R SULLIVAN

JAYCOR
ATTN: R POLL

JOHNS HOPKINS UNIVERSITY
ATTN: R MAURER

JOHNS HOPKINS UNIVERSITY
ATTN: G MASSON

KAMAN SCIENCES CORP
ATTN: DIR SCIENCE & TECH DIV
ATTN: J ERSKINE

KAMAN SCIENCES CORP
ATTN: DASIAC
ATTN: E CONRAD

KAMAN SCIENCES CORPORATION
ATTN: TECH LIB FOR/D PIRIO

KAMAN SCIENCES CORPORATION
ATTN: DASIAC
ATTN: R RUTHERFORD

KEARFOTT GUIDANCE AND NAVIGATION CORP
ATTN: J D BRINKMAN
ATTN: R SPIENGEL

LITTON SYSTEMS INC
ATTN: F MOTTER
ATTN: S MACKEY

LOCKHEED MISSILES & SPACE CO, INC
ATTN: F JUNGA
ATTN: REPORTS LIBRARY

LOCKHEED MISSILES & SPACE CO, INC
ATTN: B KIMURA
ATTN: E HESSEE
ATTN: J C LEE
ATTN: J CAYOT
ATTN: L ROSSI
ATTN: P BENE
ATTN: S TAIMUTY

LTV AEROSPACE & DEFENSE COMPANY
2 CYS ATTN: LIBRARY

MARTIN MARIETTA CORP
ATTN: J TANKE
ATTN: W BRUCE
ATTN: TIC/MP-30

MARTIN MARIETTA CORP
ATTN: S BUCHNER
ATTN: T DAVIS

MARTIN MARIETTA DENVER AEROSPACE
ATTN: P KASE
ATTN: RESEARCH LIBRARY

MARYLAND, UNIVERSITY OF
ATTN: H C LIN

MCDONNELL DOUGLAS CORP
ATTN: A P MUNIE
ATTN: R L KLOSTER

MCDONNELL DOUGLAS CORPORATION
ATTN: P ALBRECHT
ATTN: TECHNICAL LIBRARY

MESSENGER, GEORGE C
ATTN: G MESSENGER

MISSION RESEARCH CORP
ATTN: C LONGMIRE

MISSION RESEARCH CORP
2 CYS ATTN: D R ALEXANDER
2 CYS ATTN: E W ENLOW
2 CYS ATTN: R L PEASE

MISSION RESEARCH CORP
ATTN: J LUBELL
ATTN: R CURRY
ATTN: W WARE

MISSION RESEARCH CORP, SAN DIEGO
ATTN: J RAYMOND
ATTN: V VAN LINT

MITRE CORPORATION
ATTN: J R SPURRIER
ATTN: M FITZGERALD

MOTOROLA, INC
ATTN: A CHRISTENSEN

MOTOROLA, INC
ATTN: C LUND
ATTN: L CLARK

NATIONAL SEMICONDUCTOR CORP
ATTN: F C JONES

NORDEN SYSTEMS, INC
ATTN: N RIEDERMAN
ATTN: TECHNICAL LIBRARY

NORTHROP CORP
ATTN: A BAHRAMAN

NORTHROP CORPORATION SYSTEMS DIVISION
ATTN: E KING

PACIFIC-SIERRA RESEARCH CORP
ATTN: H BRODE

R & D ASSOCIATES
ATTN: D CARLSON

RAND CORP
ATTN: C CRAIN

RAND CORP
ATTN: B BENNETT

RAYTHEON CO
ATTN: H FLESCHER

RCA CORPORATION
ATTN: G BRUCKER
ATTN: V MANCINO

RESEARCH TRIANGLE INSTITUTE
ATTN: M SIMONS

ROCKWELL INTERNATIONAL CORP
ATTN: T YATES

ROCKWELL INTERNATIONAL CORP
ATTN: A BELL
ATTN: D KONO
ATTN: V DE MARTINO
ATTN: V STRAHAN
ATTN: YIN-BUTE YU

S-CUBED
ATTN: J KNIGHTEN
ATTN: J M WILKENFELD
ATTN: M ROSE

SCIENCE APPLICATION INTL CORP
ATTN: P ZIELIE

SCIENCE APPLICATIONS INTL CORP
ATTN: D LONG
ATTN: D MILLWARD
ATTN: D STROBEL
ATTN: JAMES SPRATT
ATTN: R FITZWILSON
ATTN: R J BEYSTER
ATTN: V ORPHAN
ATTN: V VERBINSKI

SCIENCE APPLICATIONS INTL CORP
ATTN: J RETZLER

SCIENCE APPLICATIONS INTL CORP
ATTN: W CHADSEY

SCIENTIFIC RESEARCH ASSOC, INC
ATTN: H GRUBIN

SUNDSTRAND CORP
ATTN: C WHITE

SYSTRON-DONNER CORP
ATTN: J RAY

TELEDYNE BROWN ENGINEERING
ATTN: G R EZELL

TELEDYNE SYSTEMS CO
ATTN: R SUHRKE

TEXAS INSTRUMENTS, INC
ATTN: E JEFFREY
ATTN: T CHEEK

TRW INC
ATTN: A WITTELES
ATTN: C BROOKS
ATTN: C E WULLER
ATTN: D AUSHERMAN
ATTN: M TAYLOR
ATTN: P GUILFOYLE
ATTN: R VON HATTEN
ATTN: TECH INFO CTR,DOC ACQ

TRW SPACE & DEFENSE SYSTEMS
ATTN: D M LAYTON

TRW SPACE & DEFENSE, DEFENSE SYSTEMS
ATTN: C BLASNEK
ATTN: DR D R GIBSON

UNISYS CORPORATION-DEFENSE SYSTEMS
ATTN: P MARROFFINO

VISIDYNE, INC
ATTN: C H HUMPHREY
ATTN: W P REIDY

FOREIGN

FOA 2
ATTN: B SJOHOLM

FOA 3
ATTN: T KARLSSON